LA-7200-PR
Progress Report

C.3

Applied Nuclear Data Research and Development

October 1—December 31, 1977

los alamos
scientific laboratory
of the University of California
LOS ALAMOS, NEW MEXICO 87545

UNITED STATES
DEPARTMENT OF ENERGY
CONTRACT W-7405-ENG. 36

The four most recent reports in this series, unclassified, are LA-6754-PR, LA-6893-PR, LA-6971-PR, and LA-7066-PR.

This work was performed under the auspices of the Nuclear Regulatory Commission, the Electric Power Research Institute, and the US Department of Energy's Divisions of Military Application, Reactor Development and Demonstration, Physical Research, and Magnetic Fusion Energy.

LA-7200-PR
Progress Report
Special Distribution
Issued: April 1978

los alamos
scientific laboratory
of the University of California
LOS ALAMOS, NEW MEXICO 87545

Applied Nuclear Data Research and Development

October 1—December 31, 1977

Compiled by

C. I. Baxman
P. G. Young

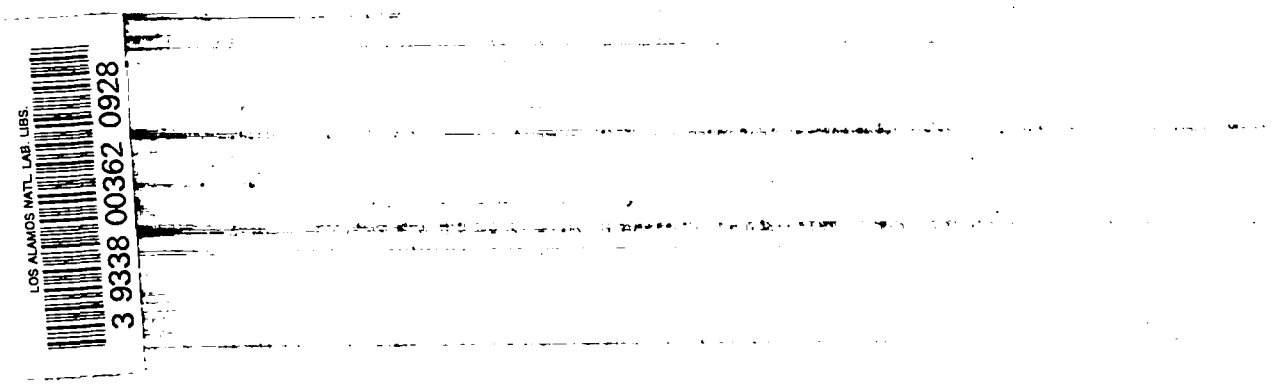

CONTENTS

APPLIED NUCLEAR DATA RESEARCH AND DEVELOPMENT
QUARTERLY PROGRESS REPORT
October 1 - December 31, 1977

Compiled by

C. I. Baxman and P. G. Young

ABSTRACT

This progress report describes the activities of the Los Alamos Nuclear Data Group for the period October 1 through December 31, 1977. The topical content is summarized in the contents.

I. THEORY AND EVALUATION OF NUCLEAR CROSS SECTIONS

A. Study of the ^{5}Li System (D. C. Dodder and G. M. Hale)

The charge symmetric 5-nucleon systems ^{5}Li and ^{5}He are the compound states of several practically important reactions [e.g., the important fusion reaction $T(d,n)^{4}He$], and consequently have been the subjects of extensive experimental study. We have been engaging in a continuing theoretical study of these systems both to achieve a greater understanding of the physics of the processes and to be able to make accurate quantitative predictions of the interesting reactions.

The study of the ^{5}Li system by means of R-matrix analysis is now involving four channels, p + ^{4}He, d + ^{3}He, P + ^{4}He*, and $\bar{d}$ + ^{3}He, where ^{4}He* is the first excited (0^{+}) state of ^{4}He, and $\bar{d}$ is the singlet (0^{+}) deuteron. The P + ^{4}He* channel is directly involved in explaining the experiment of Schroder et al.,[1] who find evidence for a $3/2^{-}$ level that is predominantly a single-particle p-wave proton interacting with the ^{4}He* cluster. Our analysis finds a similar interpretation, and quantitatively explains all the results of Schroder et al. The inclusion of the $\bar{d}$ + ^{3}He channel has similarly led to the tentative identification of a new $J = 1/2^{+}$ level that is predominantly a single-particle s-wave singlet deuteron interacting with a ^{3}He nucleus. Both of these levels manifest themselves not only in those outgoing channels that correspond to their cluster structure, but also in the primary p + ^{4}He or d + ^{3}He channels that contain most

of the experimental information. These two levels are in addition to the many levels, some firm and some still tentative, that we have previously found and which are allowing an increasingly accurate fit to the extensive body of data.

B. Resonance Model for Three-Body Final States (G. M. Hale)

Because many light nuclei have low thresholds for two-body disintegration, reactions among light nuclei in which three particles are produced become important at relatively low energies. Quite often strong resonances exist between one or more pairs of the three final-state particles. Starting from the three-body Schroedinger equation, we have derived an expression for the transition amplitude, assuming that the relative wave functions for pairs of final-state particles are dominated by single resonances, which allows us to calculate three-body spectra in terms of known parameters for the two-body resonances.

Consider the three-particle final state to be described in the coordinate system shown in Fig. 1. The relative coordinate $\underline{x}_1$ between particles 2 and 3 is conjugate to the center-of-mass momentum $\underline{q}_1$ of the 2-3 system, and the coordinate $\underline{r}_1$, locating particle 1 relative to the center-of-mass of the 2-3 system, is conjugate to momentum $\underline{k}_1$. If the 2-3 system is assumed to be the resonating pair, then the three-body transition amplitude can be expressed as

$$T^{(3)}_{\underline{q}_1\underline{k}_1\underline{k}_0} = C_{\lambda\underline{q}_1}\, T^{(2)}_{\lambda\underline{k}_1\underline{k}_0} \quad , \tag{1}$$

where

$$C_{\lambda\underline{q}_1} = \left(\frac{\hbar^2}{2\pi\mu_1 q_1}\right)^{1/2} \frac{\Gamma_\lambda^{1/2}}{\varepsilon_\lambda + \Delta_\lambda - \varepsilon_{q_1} - 1/2\ i\ \Gamma_\lambda}\, e^{-i\phi_\ell}\, Y^0_\ell(\hat{q}) \quad , \tag{2}$$

and $T^{(2)}_{\underline{k}_1\underline{k}_0}$ is the transition amplitude for the pseudo two-body process in which the projectile, incident with momentum $\hbar\underline{k}_0$, reacts to form the 2-3 pair in the resonant state $|\lambda)$, relative to which particle 1 has momemtum $\hbar\underline{k}_1$. The coefficient $C_{\lambda\underline{q}_1}$ contains the parameters of the resonant state:

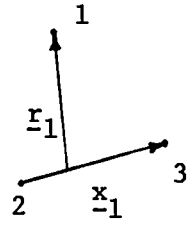

Fig. 1.
Coordinate system used to describe the three-particle final state.

$\Gamma_\lambda = 2P_\ell \gamma_\lambda^2$, where γ_λ is the reduced width amplitude, P_ℓ the penetrability.

ε_λ = the energy eigenvalue of the resonance.

$\Delta_\lambda = \gamma_\lambda^2 (S_\ell - B)$, where S_ℓ is the shift function, B the boundary condition.

ϕ_ℓ = the hard-sphere phase shift.

$Y_\ell^0 (\hat{q}_1)$ expresses the angular dependence of the resonant state.

$\varepsilon_{q_1} = \dfrac{\hbar^2 k_1^2}{2\mu_1}$, where λ_1 is the reduced mass of the 2-3 pair.

The emission spectrum for particle 1, say, is obtained from integrating essentially the square of $T^{(3)}_{\underline{q}_1 \underline{k}_1 \underline{k}_0}$ with the appropriate phase-space factor over the angles of $\underline{q}_1$. This gives spectra of the form

$$\frac{d\sigma}{d\varepsilon_{k_1} d\Omega_{k_1}} \sim \frac{1}{k_0^2} \frac{\Gamma_\lambda}{(\varepsilon_\lambda + \Delta_\lambda + \varepsilon_{k_1} - \varepsilon)^2 + 1/4\ \Gamma^2}$$

$$\times \sum_{\ell_1 \ell_0} P_{\ell_1}(k_1) P_{\ell_0}(k_0) |\bar{R}_{\ell_1 \ell_0}(\varepsilon)|^2 b_L(\ell_0 \ell_1) Y_L^0(\hat{k}_1) \quad , \qquad (3)$$

where $\bar{R}_{\ell_1 \ell_0}$ is generally a slowly varying function of the total center-of-mass energy ε, and $b_L(\ell_0 \ell_1)$ is primarily determined by Raccah coefficients for the initial and final states of the pseudo two-body reaction.

If the resonating pair includes the detected particle (say, for definiteness, that it is the 1-2 system), then the three-body amplitude has the same form as before when expressed in the $(\underline{x}_3, \underline{r}_3)$ coordinate system, where $\underline{x}_3$ is the relative coordinate for particles 1 and 2, and $\underline{r}_3$ is the coordinate for particle 3 relative to the center-of-mass of the 1-2 system. That is,

$$T^{(3)}_{\underline{q}_3 \underline{k}_3 \underline{k}_0} = C_{\lambda q_3} T^{(2)}_{\lambda \underline{k}_3 \underline{k}_0} \quad ,$$

where $(\underline{q}_3\underline{k}_3)$ are the momenta conjugate to $(\underline{x}_3,\underline{r}_3)$. However, because now q_3 and k_3 depend on the angle of $\underline{q}_1$, the integration over q_1 becomes considerably more complicated. An analytic expression can be obtained in the case of an uncharged, s-wave interaction, both between the resonating pair, and between particle 3 and the 1-2 system, if the energy dependence of Γ_λ is ignored in the denominator of $C_{\lambda q_3}$. The spectrum in this case has the form

$$\frac{d\sigma}{d\epsilon_{k_1} d\Omega_{k_1}} \sim \frac{1}{k_0^2} P_{\ell_0}(k_0) |\bar{R}_{0\ell_0}(\epsilon)|^2 \frac{1}{k_1 q_1} \sum_{\ell} (2\ell+1) |Q_\ell(z)|^2 \quad , \qquad (4)$$

where again $R_{0\ell_0}(\epsilon)$ is a slowly varying function of ϵ, and Q_ℓ is the irregular Legendre polynomial having complex argument

$$z = \frac{m_{12}m_{23}(\epsilon_r - 1/2\ i\Gamma) - m_1 m_3 \epsilon - (m_{12}m_{23} - 2m_1 m_3)\epsilon_{k_1}}{M q_1 k_1} \quad .$$

Here, ϵ_r and Γ are the resonant energy and width of the resonance in the 1-2 system, and the mass factors

$$m_{ij} = m_i + m_j \quad , \qquad M = \sum_{i=1}^{3} m_i \quad .$$

We have applied these expressions to the calculation of inelastic neutron spectra resulting from neutron bombardment of ^{6}Li. Only two resonance configurations of the (n,α,d) final state were taken into account: the d-wave α-d resonance that forms ^{6}Li*(3+,2.185) and the lowest p-wave n-α resonance that forms ^{5}He(3/2$^-$,g.s.). The coupling in both cases to the n-^{6}Li channel was assumed to be only in the 3/2$^-$ state, because a resonance occurs in this state at energies close to the three-body threshold. The calculated differential neutron spectrum at 90° for an incident energy of 5 MeV is shown in Fig. 2. The results of Eqs. (3) and (4) have been transformed to the laboratory system in which most of the measurements are expressed. The spectrum resembles the data of Hopkins, Drake,

and Condé,[2] although the points shown in the inelastic peak for this measurement are uncorrected for multiple scattering, attenuation, and resolution effects. Presumably, these effects are responsible for the differences in width between the measurements and the calculations for the inelastic peak. The lack of neutrons at the high-energy end of the spectrum is reproduced much better in the present calculation than in three-body phase-space considerations.

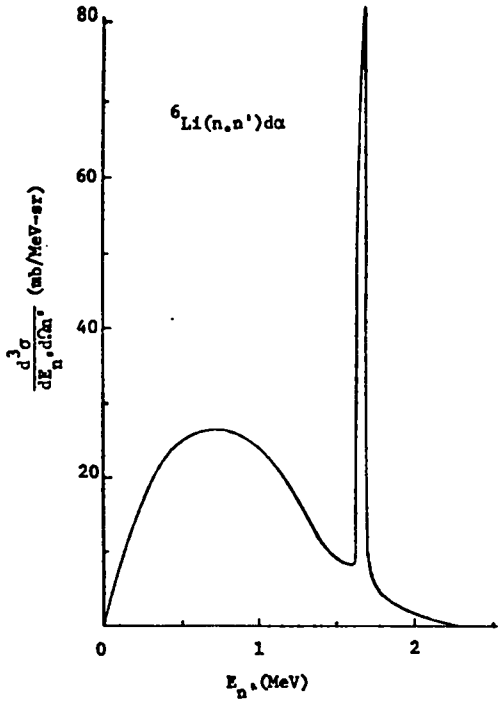

Fig. 2.
Calculated spectrum in the laboratory system for neutrons detected at 90°, with 5 MeV neutrons incident.

C. Spectrum Averaged Hydrogen and Helium Production Cross Sections (D. W. Muir E. D. Arthur, R. J. Barrett, and P. G. Young)

Neutron-induced hydrogen and helium production cross sections for carbon, nitrogen, oxygen, and magnesium as well as isotopes of these elements have been obtained for a fast-neutron spectrum typical of the Oak Ridge Reactor (ORR). Spectrum-averaged and thermal results are given in Table I for both the element and its isotopes where the reaction of interest had a threshold far enough below 8 MeV to be of importance. Several methods were used to produce the energy-dependent cross sections that werethen averaged over the ORR spectrum using the processing code NJOY. In Table I, entries marked "ENDF/B" were obtained through use of evaluated neutron data appearing in the ENDF/B-IV system. For results marked "experimental" a smooth curve was drawn through available experimental data to produce the energy-dependent cross sections. Hauser-Feshbach statistical model calculations were made for the $^{17}O(n,x\alpha)$ and $^{26}Mg(n,\alpha)$ cross sections. Entries noted as "estimated" were obtained from an analysis of the systematics of (n,p) and (n,α) reactions[3] in this mass region. Finally, those marked "experimental spectrum" represent spectrum-averaged cross sections determined experimentally for the Kyoto University Reactor spectrum,[4] which is similar in shape to the ORR spectrum between 1 and 8 MeV.

TABLE I

THERMAL VALUES AND SPECTRUM-AVERAGED CROSS SECTIONS (0.1→12 MeV)

Reaction	Thermal X-Sec. (b)	Spectrum-Averaged X-Sec. (b)	Method
$^{12}C(n,\alpha)$		1.27-3	ENDF/B
$^{12}C(n,n\alpha)$		3.59-4	ENDF/B [(n,n3α) x 3]
$^{13}C(n,\alpha)$		8.59-3	Estimated
$^{14}N(n,p)$	1.81 ± .05	3.58-2	ENDF/B
$^{14}N(n,d)$		3.67-4	ENDF/B
$^{14}N(n,t)$		1.02-3	ENDF/B
$^{14}N(n,\alpha)$		9.65-2	ENDF/B
$^{16}O(n,\alpha)$		1.10-2	ENDF/B
$^{17}O(n,\alpha)$	.235 ± .01	.105	Calculated
$^{17}O(n,n\alpha)$		1.59-3	Calculated
$^{18}O(n,\alpha)$		3.79-4	Estimated
$^{Nat}Mg(n,p)$		1.35-3	ENDF/B
$^{Nat}Mg(n,\alpha)$		3.48-3	ENDF/B
$^{24}Mg(n,p)$		1.47-3	Experimental
$^{24}Mg(n,\alpha)$		5.55-4	Estimated
$^{25}Mg(n,p)$		1.39-3	Estimated
$^{25}Mg(n,\alpha)$	Not Available	2.83-2	Estimated from ENDF/B
$^{26}Mg(n,\alpha)$		0.	Calculated
$^{27}Al(n,p)$		4.94-3	ENDF/B
$^{27}Al(n,\alpha)$		7.50-4	ENDF/B
$^{Nat}Si(n,p)$		8.07-3	ENDF/B
$^{Nat}Si(n,\alpha)$		3.46-3	ENDF/B
$^{28}Si(n,p)$		6.68 ± .08-3	Experimental and Exp. Spectrum
$^{28}Si(n,\alpha)$		4.70-3	Experimental
$^{29}Si(n,p)$		2.9 ± .1-3	Experimental Spectrum
$^{29}Si(n,\alpha)$		6.24-3	Estimated
$^{30}Si(n,\alpha)$		1.3 ± .2-4	Experimental Spectrum

D. Calculation of Zirconium Cross Sections (P. G. Young and E. D. Arthur)

Calculations of neutron-induced reaction cross sections on ^{88}Zr from 4 to 16 MeV and ^{89}Zr and ^{90}Zr between 4 and 20 MeV have been made using the GNASH nuclear-model code and global-parameter sets. The global-optical parameter sets used were Wilmore-Hodgson[5] (neutrons), Perey[6] (protons), and McFadden-Satchler[7] (alphas). The Brink-Axel[8] giant-dipole resonance model was used to provide the energy dependence for the gamma-ray transmission coefficients. The calculated results are tabulated in Table II.

For the cases of n + ^{88}Zr and n + ^{89}Zr reactions, where proton binding energies in the compound nuclei ^{88}Zr and ^{89}Zr are several MeV less than for neutrons, the calculated results are somewhat sensitive to the amount of gamma-ray competition that, in turn, is influenced by the normalization of the gamma-ray strength function. Also, optical-model parameters for sub-Coulomb protons are very poorly known, and recent experimental results[9] indicate anomalies in proton optical-model parameters for low-energy protons in this mass region. These effects combine to increase uncertainty in calculations of this nature, and further study is required to resolve these problems.

E. Calculations of $^{191}Ir(n,\gamma)$ and $^{193}Ir(n,\gamma)$ Cross Sections (E. D. Arthur and O. Bersillon (Service de Physique Nucléaire, Bruyères-le-Châtel, France)

Statistical-model calculations of the ^{191}Ir (37.6%) and ^{193}Ir (62.4%) neutron capture cross sections have been made in the energy range from 250 eV to 6 MeV. Below 1 MeV the calculations were made using the COMNUC statistical code, assuming only E1 contributions and that all gamma rays resulted from capture. Correlation and width fluctuation corrections were included for this portion of the calculation. From 1 to 6 MeV, gamma-ray cascades become important and the GNASH code, which includes a full treatment of these cascades, was used. Cascades were allowed by E1, M1, and E2 transitions. In both COMNUC and GNASH the gamma-ray strength function was assumed to have the energy dependence given by the Weisskopf[10] approximation, which was normalized to experimental values for the ratio of the average gamma-ray width $\langle\Gamma\gamma\rangle$ to the observed s-wave spacing $\langle D\rangle$. Values for these quantities were taken from BNL-325[11] and are shown in Table III.

Special care was taken in the determination of neutron-optical parameters needed to generate neutron transmission coefficients. The spherical parameters of Auerbach[12] were found to give a good fit to the total cross section from 0.001

TABLE II

CALCULATED Zr CROSS SECTIONS (b)

E_n (MeV)	(n,γ)	(n,n')[a]	(n,p)	(n,α)	(n,2n)	(n,np)	(n,nα)	(n,pn)	(n,αn)
n + ^{88}Zr									
4	1.66-3	1.728	0.103	4.9-5					
6	7.9-4	1.541	0.14	5.5-4					
8	4.4-4	1.563	0.156	1.9-3					
9	3.2-4	1.542	0.152	3.1-3					
10	2.3-4	1.506	0.148	4.7-3		1.4-4			
11	1.7-4	1.461	0.143	7.2-3		4.3-3		7.0-4	
12	1.3-4	1.395	0.136	1.06-2		2.9-2	4.1-6	4.8-3	
13	1.0-4	1.258	0.123	1.5-2	5.1-2	8.3-2	4.0-5	1.6-2	1.3-5
14	8.4-5	1.055	0.107	2.03-2	0.186	0.127	1.6-4	3.2-2	1.3-4
15	7.1-5	0.903	0.091	2.65-2	0.293	0.156	4.4-4	5.0-2	4.9-4
16	6.1-5	0.747	0.08	3.29-2	0.429	0.161	8.2-4	6.5-2	1.6-3
n + ^{89}Zr									
20		0.068	0.0541	0.0554	1.175	0.1388		0.0823	
18		0.097	0.0595	0.0407	1.134	0.2250		0.0664	
16		0.170	0.0686	0.0281	0.9125	0.4226		0.0464	
14		0.377	0.0841	0.0169	0.6371	0.5178		0.0203	
13		0.606	0.0888	0.0125	0.5083	0.4355		0.0114	
12		0.968	0.0933	0.0089	0.3191	0.2898		0.0037	
11.5		1.176	0.0940	0.0073	0.2332	0.1857		0.0018	
11		1.385	0.0941	0.0059	0.1371	0.0908		0.0006	
10.5		1.535	0.0935	0.0047	0.0781	0.0206		0.00022	
10		1.628	0.0928	0.0037		0.0053		1.5-5	
8		1.744	0.0871	0.0011					
6		1.820	0.0729	0.00032					
4		1.834	0.0896	0.00012					
n + ^{90}Zr									
20		0.237	0.0342	0.0404	1.157	0.0589		0.0453	
18		0.346	0.0343	0.0266	1.116	0.0695		0.0283	
16		0.558	0.0328	0.0151	0.9439	0.0837		0.0131	
15		0.723	0.0306	0.0105	0.8050	0.0731		0.0072	
14		0.998	0.0274	0.0069	0.5504	0.0670		0.0031	
13		1.402	0.0230	0.0041	0.1710	0.0613		0.00088	
12.5		1.601	0.0205	0.0031		0.0457		0.00039	
10		1.741	0.0094	0.00049		2.3-5			
8		1.828	0.0043	9.6-5					
6		1.889	0.0019	1.0-5					
5		1.920	0.0098	1.6-6					
4		1.919	0.00029	2.5-7					

[a] CE removed.

to 15 MeV and also agreed with experimental values for s- and p-wave strengths and for the potential scattering radius R', as shown in Table IV.

In these calculations, 18, 6, 17, and 9 discrete levels were used for ^{191}Ir, ^{192}Ir, ^{193}Ir, and ^{194}Ir, respectively. Above these discrete levels, the Gilbert-Cameron[13] level density expression (with Cook[14] parameters) was used with the constant temperature portion matched to experimental information concerning known levels.

The calculated results are compared in Figs. 3 and 4 to available experimental data for ^{191}Ir and ^{193}Ir (n,γ) reactions between 0.005 and 3 MeV. For ^{191}Ir the calculations agree with both the recent Drake[15] results and the older Nagle[16] measurements. For ^{193}Ir the present calculations are somewhat lower than most experimental data points but agree again with the Drake values. The calculated results were combined isotopically and are compared with experimental data for capture on natural Ir in Fig. 5.

In the future we plan to extend the present calculations up to 20 MeV taking into account giant-dipole resonance effects that occur in the neutron-energy range from 10 to 14 MeV. Also, because the Ir isotopes are somewhat deformed ($B_2 \approx 0.14$), we plan to repeat these calculations using neutron transmission coefficients from the coupled channels optical model program JUPITOR.

TABLE III

GAMMA-RAY STRENGTH NORMALIZATION PARAMETERS

	n + ^{191}Ir	n + ^{193}Ir
$\langle\Gamma_\gamma\rangle$ (eV)	0.081 ± 0.01	0.094 ± 0.02
$\langle D\rangle$ (eV)	3.3 ± 0.8	7.7 ± 0.8
$2\pi\langle\Gamma_\gamma\rangle$ (adopted)	0.154	0.0734

TABLE IV

EXPERIMENTAL AND CALCULATED S_0, S_1, and R' VALUES

	^{191}Ir		^{193}Ir	
	Experimental	Calculated	Experimental	Calculated
$10^4\ S_0$	2.2 ± 0.2	2.21	2.0 ± 0.2	2.12
$10^4\ S_1$	0.2 - 0.8	0.85	0.2 - 0.8	0.88
R' (fm)	8.6	8.79	8.6	8.79

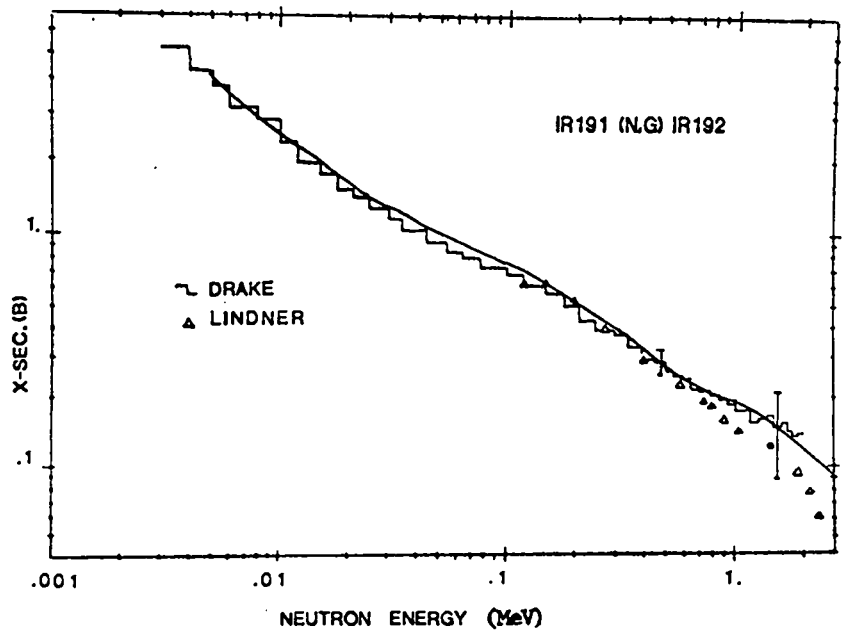

Fig. 3.
^{191}Ir calculated and experimental (n,γ) cross sections.

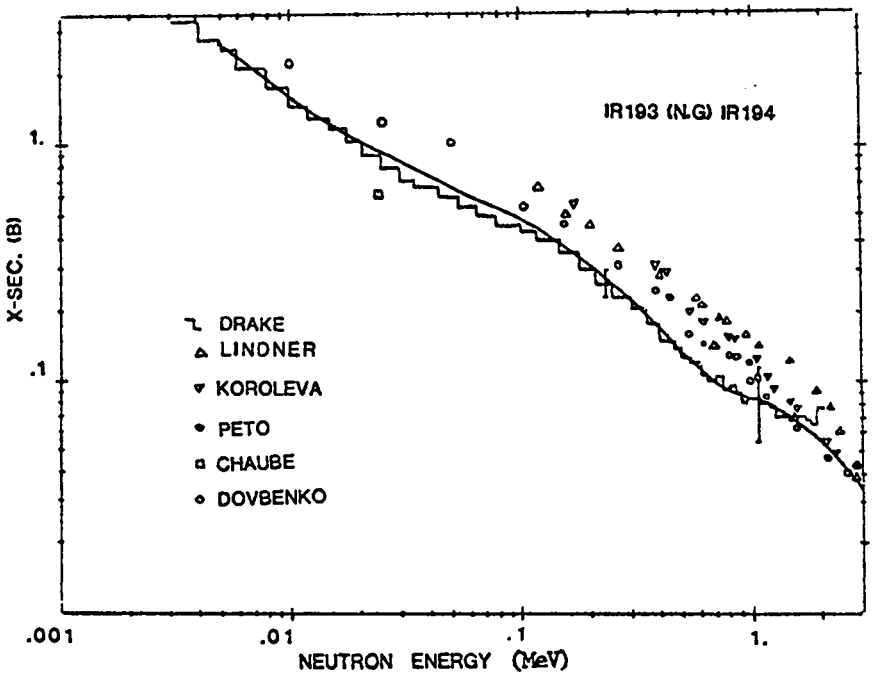

Fig. 4.
Experimental and calculated results for the ^{193}Ir (n,γ) reaction.

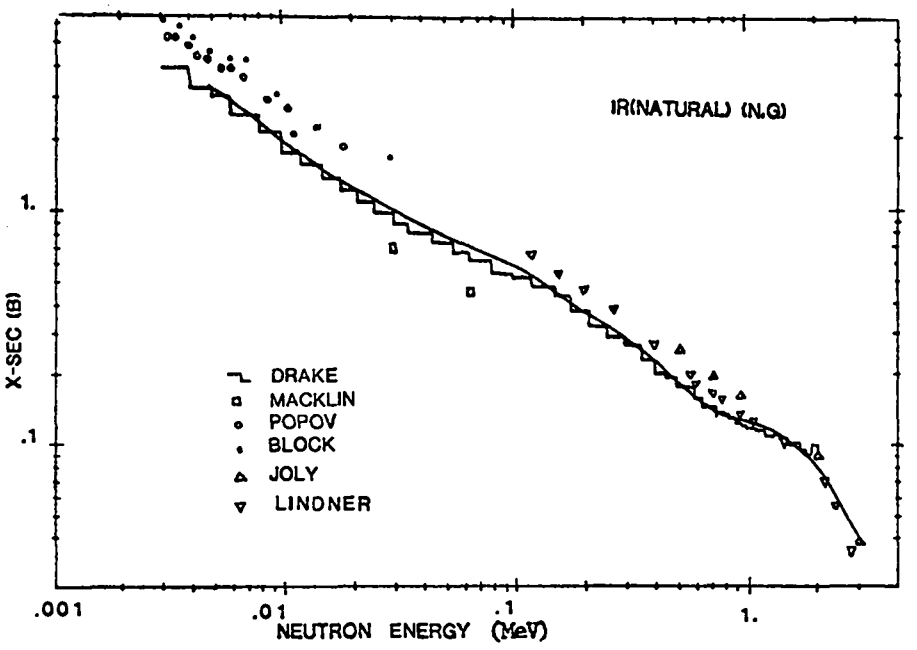

Fig. 5.
Comparison of experimental and calculated neutron capture cross sections on natural Ir.

F. Modification of the Preequilibrium Programs PRECO-A and PRECO-B (O. Bersillon, Service de Physique Nucleaire, Bruyeres-le-Chatel, France)

In order to improve the preequilibrium portion of the preequilibrium statistical model code GNASH,[17] we plan to incorporate one of the Kalbach master equation preequilibrium programs PRECO-A or PRECO-B[18] into GNASH. However, because both of these programs consist of one large routine that is somewhat unwieldly, we have rewritten them by introducing several subroutines for each main step of the preequilibrium calculation. Thus, separate subroutines exist for transition and emission rate calculations, for solution of the master equation set by finite difference methods, and for calculations of the emitted particle spectra. These modifications resulted in a decrease in the computer time needed to run these programs by approximately a factor of 2.

G. Calculations for ^{233}U Preliminary ENDF/B-V Evaluation (D. G. Madland and P. G. Young)

A series of cross-section calculations have been performed for use in a preliminary ^{233}U evaluation by the Los Alamos Scientific Laboratory (LASL) Theoretical Group, T-2. Total, elastic, inelastic, fission, capture, (n,2n), and (n,3n) cross sections were calculated on energy grids of, at most, 207 points ranging from 50 keV to 20 MeV. Combined direct- and compound-elastic spherical

optical-model calculations, direct coupled channel inelastic calculations, and Hauser-Feshbach statistical-model calculations were performed for the various reactions at the appropriate energy ranges. Several effects, however, were neglected in this first calculation because of the deadline involved. For example, inelastic scattering to members of excited rotational bands, semidirect effects, and direct-capture calculations will have to be included in future calculations. A summary of the present calculations follows.

The calculational effort began with the development of a global neutron-nucleus spherical-optical potential for the uranium isotopes. Thirty-two sets of total cross-section data together with resolved and unresolved elastic-angular distribution data were simultaneously fit using a global optical-model search code. For low-energy ($\lesssim$ 2 MeV) data, the code simultaneously optimizes the magnitude of the (assumed) isotropic compound-elastic contribution and the angular distribution absolute normalization (this is done within the loop that minimizes the total chi-square from data of all energies). Volume and surface Saxon-Woods form factors were employed. Their strengths and diffuseness were parameterized in terms of the neutron bombarding energy E_L (neutron), and the volume normalized target isospin $\eta = (N-Z)/A$. Total cross-section data used (from ^{233}U, ^{235}U, ^{238}U) ranged from 1.0 keV to 19.86 MeV, resolved-elastic angular-distribution data (from ^{235}U and ^{238}U) ranged from 0.5 to 14.1 MeV. The resultant 1 keV-20 MeV spherical-optical potential has both volume and surface absorptive terms and has a total of 15 coefficients, not counting the spin orbit term that was fixed throughout, as described in Ref. 19. The total elastic cross section predicted by the potential was used as the starting set of values in MT=2. The calculated total cross section was used in regions devoid of data for MT=1.

A coupled-channel calculation of the direct inelastic was performed by deforming the spherical global potential using the β_2 and β_4 experimental values determined by Bemis et al.[20] in (α,α') measurements on ^{234}U. The results of these calculations compose the direct parts of MT=51, MT=52, MT=53, MT=54, and MT=4.

The remaining calculations were made using the statistical model code COMNUC with the spherical global-optical potential providing all neutron-transmission coefficients. The reactions (n,γ), (n,n'), (n,2n), (n,f), (n,3n), (n,n'f), and (n,2nf) were calculated from 50 keV to 20 MeV. Twelve discrete-fission channels were used in the (n,f) calculations, and ten discrete-levels in both (n,n'f) and (n,2nf). Both low- and high-energy approximations were used in the (n,γ) calculations. Ten discrete levels were used in the (n,n') calculations. The Axel[21]

estimate was used for dipole radiation; experimental values exist for the giant-dipole resonance energy and width and were employed in this calculation. The Gilbert and Cameron[13] level density description was used throughout. Good agreement was obtained with the experimental total and fission cross sections. The agreement with the experimental capture cross sections was acceptable. Results from these calculations were used for the reaction types MT=4, MT=16, MT=17, MT=51 through 54, and MT=91.

H. Preliminary Evaluation of the Neutron-Induced Reactions for ^{233}U (L. Stewart, D. G. Madland, and P. G. Young)

The $^{233}U/^{232}Th$ fuel cycle for fast-reactor applications is currently under study. While the evaluated nuclear data for thermal applications have been periodically updated, the fast-neutron energy region for these nuclei has received little attention over the past 10 yr. Consequently, efforts are under way at several laboratories to improve the evaluated data files for the forthcoming issue of Version V of ENDF/B. At LASL a preliminary re-evaluation of the neutron-induced data for ^{233}U has recently been completed between 50 keV and 20 MeV. In addition, $\bar{\nu}_p$ and the fission spectrum have been re-evaluated over the entire energy region. This preliminary evaluation is briefly summarized below.

1. 10^{-5} eV to 20 MeV.

(a) The evaluation for $\bar{\nu}_p$ is shown in Fig. 6 up to 2 MeV. Above 2.4 MeV (not shown) the new evaluation is less than that of ENDF/B-IV, but is higher from 11 to 20 MeV. Similarly, the thermal value is lower, but the 1-MeV region is higher compared to Version IV. The evaluation for $\bar{\nu}_d$ is essentially that of Version IV.

(b) The prompt fission neutron spectrum was re-evaluated by assuming an incident energy independent Watt shape with $\bar{E}$ = 2.059 MeV.

2. Thermal and Resolved Resonance Region. The thermal and resolved resonance region was unchanged from Version IV.

3. Unresolved Region (60 eV to 10 keV). Resonance parameters were extracted at Hanford Engineering Development Laboratory (HEDL)[22] using the average cross sections of Version IV (there are indications that the total, elastic, fission, and capture cross sections should be re-evaluated in this energy range).

4. 50 keV to 20 MeV. The cross sections were re-evaluated above 50 keV and matched to Version IV below 50 keV. The evaluated total cross section (Fig. 7) is based upon the data of Green[23] and Foster[24] between 60 keV and 13.9 MeV

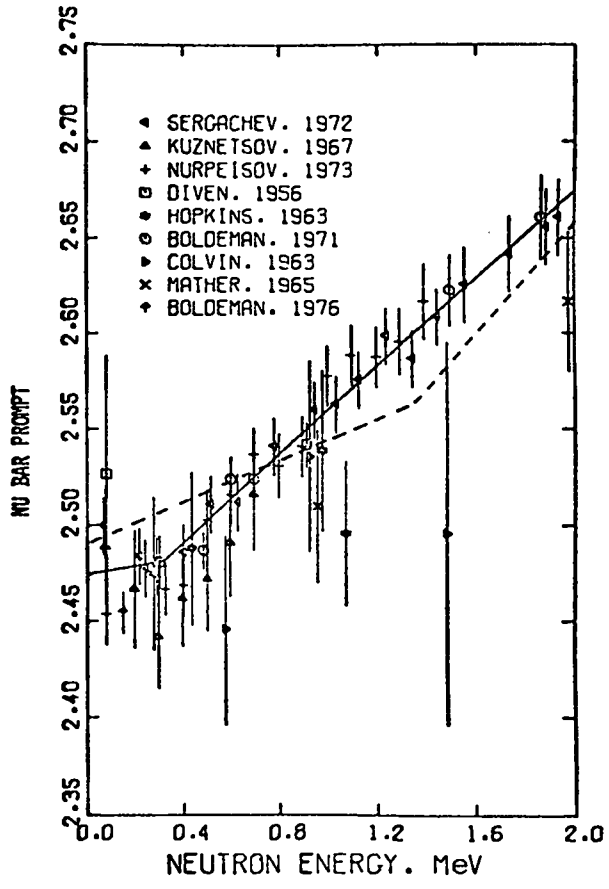

Fig. 6.
$\bar{\nu}_p$ vs neutron energy for ^{233}U; ENDF/B-IV (---), preliminary ENDF/B-V (——), and experimental measurements[25] (symbols).

and calculations using a global actinide optical potential[26] at lower and higher energies (see the previous section for a description of the calculations). The evaluated fission cross section (Fig. 8) is based primarily upon the $^{233}U/^{235}U$ ratio measurements of Behrens et al.[27] normalized to the ENDF/B-V ^{235}U fission cross section. The (n,γ) cross section is based upon the measurements of Hopkins and Diven[28] up to 1 MeV and systematics at higher energies. The elastic, inelastic, (n,2n), and (n,3n) evaluations are derived from Hauser-Feshbach statistical model, optical model, and direct coupled-channel calculations.

5. Planned Updates in the 50-keV to 20-MeV Region. Angular distributions for the elastic and direct inelastic cross sections should be calculated, additional discrete levels should be included, and semidirect effects should be introduced in order to provide more realistic inelastic-neutron spectra. The fission cross section should be decomposed into first-, second-, and third-chance fission contributions. Finally, energy distributions for (n,2n) and (n,3n) reactions should be improved. Calculations of the above are in progress.

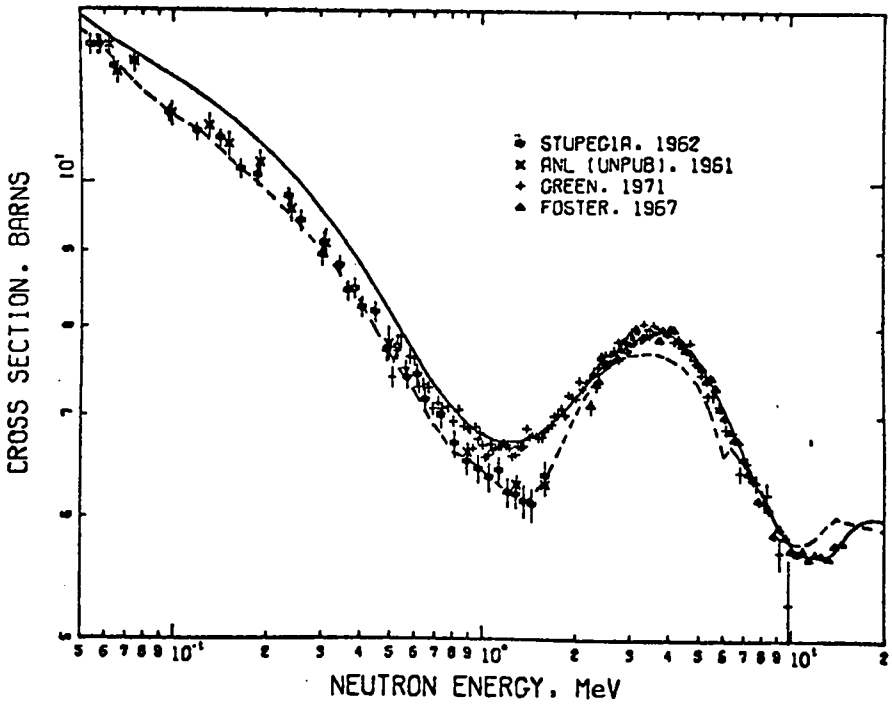

Fig. 7.
The total neutron cross section vs neutron energy for ^{233}U; ENDF/B-IV (---), preliminary ENDF/B-V (——), and experimental measurements[23-25] (symbols).

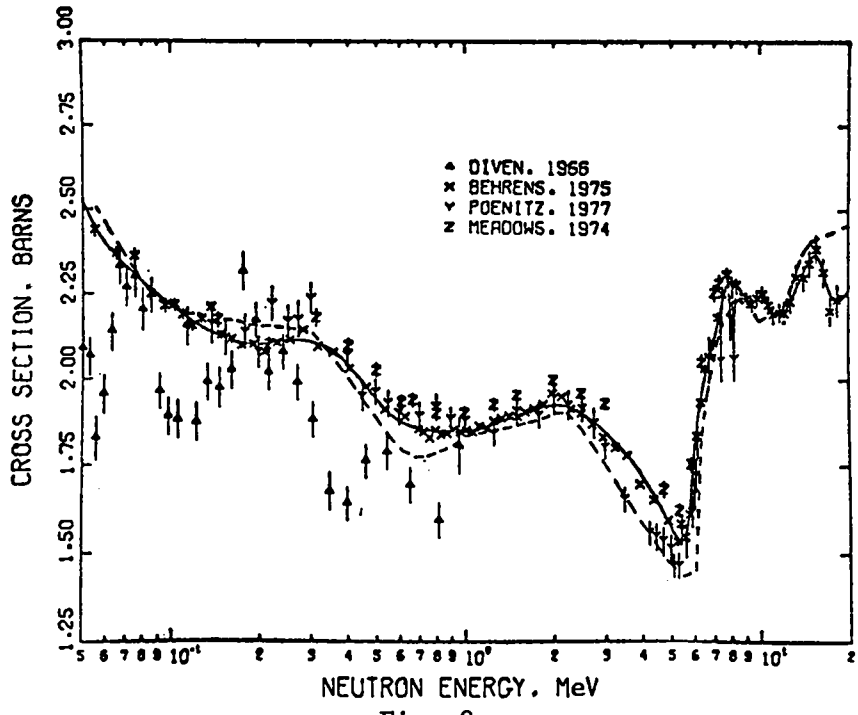

Fig. 8.
The fission cross section vs neutron energy for ^{233}U; ENDF/B-IV (---), preliminary ENDF/B-V (——), and experimental measurements[25,26] (symbols)

I. Phase I Reviews of ENDF/B-V Evaluations [E. D. Arthur, D. G. Foster, Jr., G. M. Hale, R. J. LaBauve, M. Moore (P-3), D. Muir, L. Stewart, and P. G. Young]

A number of Phase I reviews of evaluations submitted for Version V of ENDF/B have been completed or are in progress by LASL personnel. The list of materials includes ^{12}C (Hale, Stewart), F (Muir), Fe (LaBauve), Ni (Foster), Pb (Arthur), ^{235}U (Stewart), ^{242}Pu (Stewart, Young), and ^{237}Np, ^{248}Cm, ^{252}Cm (Moore, Stewart).

II. NUCLEAR CROSS-SECTION PROCESSING

A. Cross-Section Production (R. E. MacFarlane, D. W. Muir, and R. J. Barrett)

A new version of our large 30-neutron group by 12-photon group cross-section library has been completed. This version improves the heating cross sections and corrects errors in several isotopes. The results are available in both DTF and MATXS format.

The ^{12}C evaluation for preliminary ENDF/B-V has been processed for use in the LASL Monte Carlo library. Also, preliminary ENDF/B-V ^{239}Pu and ^{233}U were processed to test the evaluations and the Version V capabilities of NJOY. As a result, several corrections were made to the HEATR and MCNR modules.

B. Multigroup Cross-Section Sets for NBS [D. W. Muir, R. J. LaBauve, and G. E. Bosler (T-1)]

We have produced 53-group, 4-table multigroup cross-section sets for use in design of experiments at the Intermediate-energy Standard Neutron Field (ISNF), an irradiation facility[29] at the National Bureau of Standards (NBS). The ISNF arrangement consists of a 15-cm radius cavity in the thermal column of the NBS reactor, a 5.8-cm inner radius, 7.1-cm outer radius ^{10}B-Al spherical shell lightly supported at the cavity center, and fission source disks of ^{235}U placed symmetrically around the periphery of the cavity. The 53-group cross sections provided to NBS are space-dependent, having been generated by a group-collapse calculation using the fluxes from a 240-group ONETRAN calculation of ISNF, averaged over several different spatial regions. The group collapse was performed using the CINX[30] code, specially modified[31] to preserve the angular distributions of scattered neutrons through the use of the Legendre moments of the neutron flux in the collapse algorithm. The input 240-group cross sections for ^{12}C, ^{10}B, ^{11}B, and ^{27}Al were taken from LIB-IV-240, generated previously[32] at LASL using ENDF/B-IV evaluated data and the MINX[33] nuclear data processing code. Coarse-group sets for ^{12}C, ^{10}B, ^{11}B, and ^{27}Al were generated with CINX for the spatial regions described in Table V.

TABLE V

REGIONS USED FOR GENERATION OF
SPACE-DEPENDENT 53-GROUP CROSS SECTIONS

Inner and Outer Radii of Region (cm)	Cross-Section Set Names
14.92 - 30.00	C1530
30.00 - 45.00	C3045
14.92 - 65.00	C1565
45.00 - 65.00	C4565
5.838 - 7.131	B10-0, B11-0, A1-0
5.838 - 6.392	B10-1, B11-1, A1-1
6.392 - 6.762	B10-2. B11-2, A1-2
6.762 - 7.131	B10-3, B11-3, A1-3
7.131 - 7.201	A1-4

NBS also requested that we perform several additional 240-group ONETRAN calculations to determine the effect of small changes in Al and ^{10}B concentrations and the effect of changing the S_n quadrature on the central scalar flux. Results of these runs are shown in Figs. 9-13.

C. NJOY Code Development (R. E. MacFarlane)

Additional IBM compatibility tests performed at Oak Ridge National Laboratory (ORNL) by R. Q. Wright have resulted in several corrections to the GROUPR and CCCCR modules. Tests on preliminary ENDF/B-V evaluations revealed errors in HEATR and MCNR that have been corrected. A capability to flux average the reciprocal neutron velocity in GROUPR and write the result on the ISOTXS output of CCCCR was added. Extensive changes were made to MATXSR to simplify input and to store self-shielded cross sections using the $\Delta\sigma$ method (see Sec. II.F). Finally, code validation efforts for thermal reactor work located errors in the GROUPR flux calculator and in the THERMR coherent scattering option.

D. NJOY-MINX Comparisons (R. J. Barrett)

In February 1976, Kidman and MacFarlane released the LIB-IV[34] cross-section library. Intended for use in fast-reactor calculations, the library consisted of group averaged neutron cross sections, transfer tables, self-shielding factors, and delayed neutron yields for 101 isotopes in CCCC format (ISOTXS, BRKOXS, and DLAYXS). The library was processed using the MINX[33] code.

In order to directly compare the NJOY and MINX processing codes, a five-isotope library, processed by NJOY, has recently been produced using the same

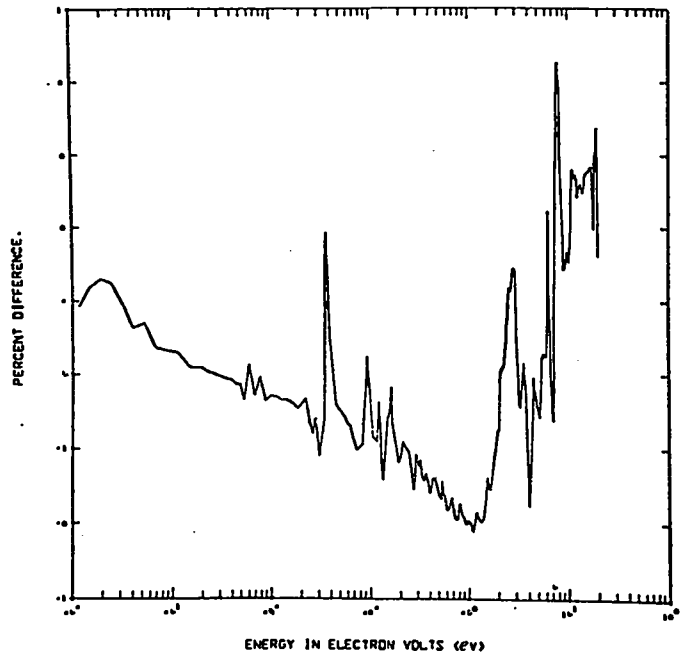

Fig. 9.
S_n quad changed to S_4. Percent difference from reference case.

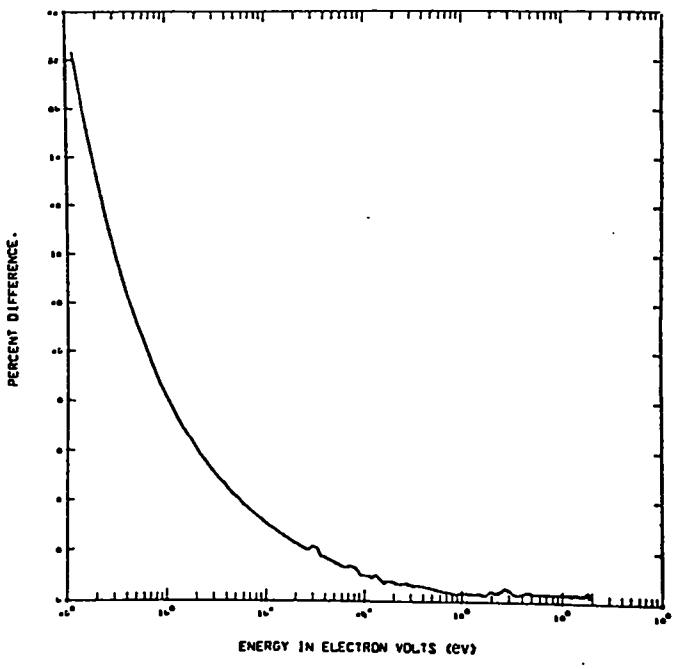

Fig. 10.
Five Percent increase in ^{10}B concentration. Percent difference from reference case.

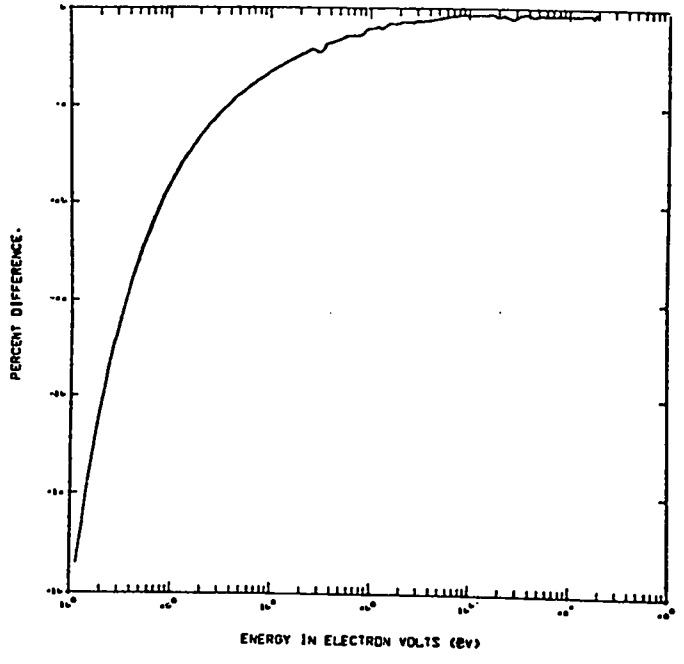

Fig. 11.
Five percent decrease in B^{10} concentration. Percent difference from reference case.

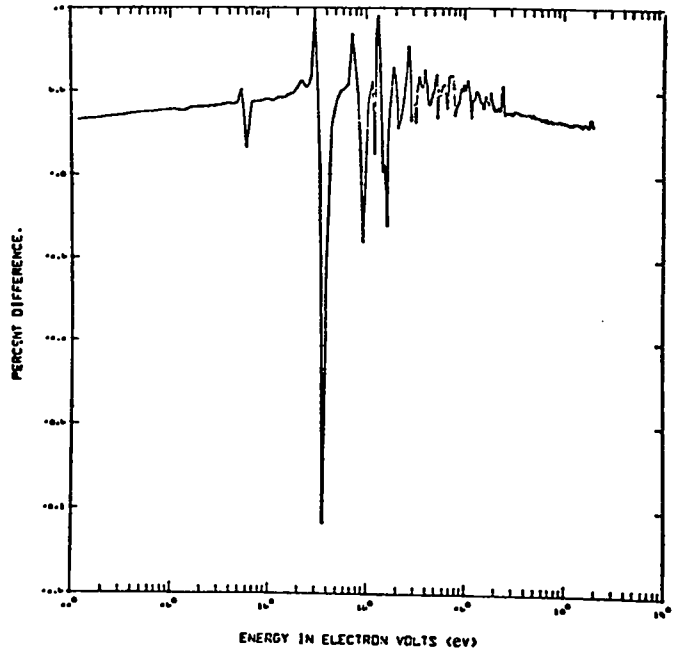

Fig. 12.
Five percent decrease in Al concentration. Percent difference from reference case.

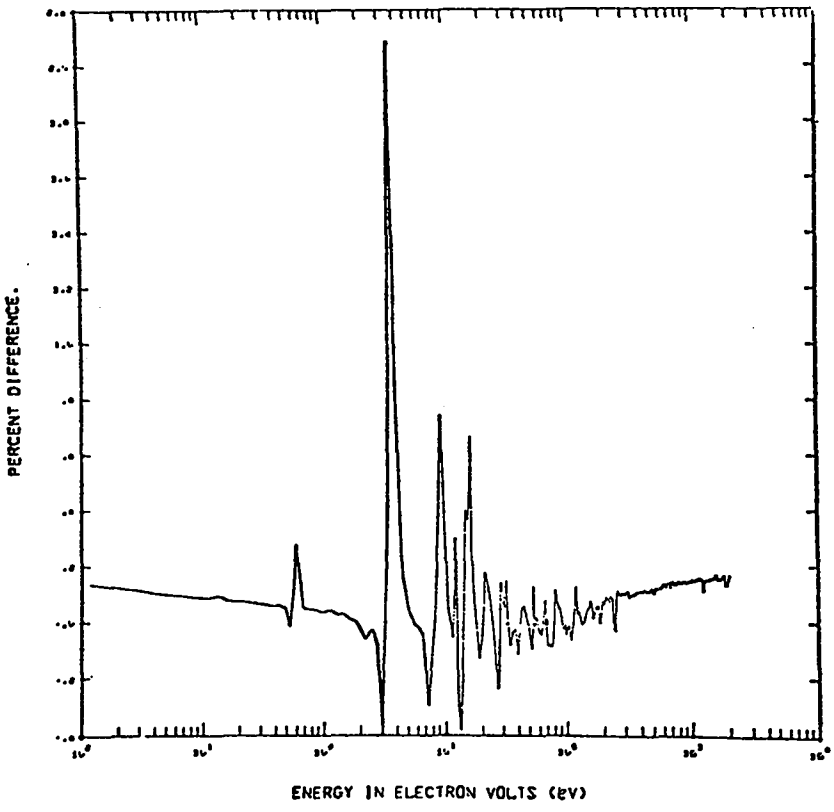

Fig. 13.
Five percent increase in Al concentration.
Percent difference from reference case.

group structure, weight function, dilution factors, temperatures, and tolerances as the corresponding isotopes in LIB-IV. A code was written to compare the two processed versions of each isotope by calculating the relative differences of each number in the respective ISOTXS and BRKOXS files (the DLAYXS file was compared by inspection). Absolute differences of less than 10^{-6} in the cross sections or self-shielding factors were ignored, as were relative differences of less than 0.01.

The first noticable difference in the two codes was the substantial reduction in running time exhibited by the NJOY code (Table VI). The total time required to perform the same task was 2.7 times greater for MINX.

As for the detailed number-by-number comparisons, no alarming discrepancies showed up. Where relative differences of more than 0.01 occurred, they tended to be of the order of a few percent. The relative differences that were larger (several tens of percent) were rare and tended to correspond to small cross-sections (or f-factor) values. This is encouraging because discrepancies in the two

TABLE VI

COMPARISON OF NJOY AND MINX RUNNING TIMES
(CDC-7600 with the CROS System)

Isotope	Running Time (s) MINX	NJOY
^{1}H	133	103
^{16}O	590	227
Fe	1192	548
^{235}U	2832	1001
^{238}Pu	1043	271
Total	5790	2150

data sets could result from differences in resonance reconstruction (resolved and unresolved), linearization, Doppler broadening, group averaging, or CCCC formatting.[35]

This study has already produced several minor modifications to NJOY, resulting in the elimination of several discrepancies. Some of the remaining differences are still a mystery to us and deserve further investigation. However, we believe that the majority of the remaining discrepancies can be explained in terms of the following well-understood differences between NJOY and MINX.

1. The prompt fission spectrum (χ) from MINX is generated from the spectrum at one incident neutron energy (1.0 MeV). NJOY produces a flux-averaged spectrum by summation of the fission matrix.

2. The total cross section in NJOY is the sum of the linearized partials, while MINX used the linearized values from MT=1 of ENDF. This advantage of NJOY leads to differences in the total cross sections, as well as the transport cross sections and f-factors.

3. The Doppler broadening in MINX has been deactivated below 0.1 eV due to numerical instabilities. Among other things, this produces large differences for low-energy elastic scattering at temperatures other than 0 K. While the NJOY cross sections exhibit the 1/v tail that is automatically produced in Doppler broadening to preserve reaction rate, the MINX cross sections are flat.

4. In NJOY, the transport cross section is defined in the approximation

$$\sigma^{g}_{tr,1} = \sigma^{g}_{t,1} - \sum_{g} \sigma_{s,1}^{(g \to g')} \quad ,$$

as recommended in the CCCC manual.[35] The MINX code used the further approximation that

$$\sigma^g_{tr,1} = \sigma^g_{t,1} - \bar{\mu}\,\sigma^g_{el,0} \quad .$$

There is no guarantee that this approximation is equivalent to the recommended one. Furthermore, the flux-weighted (P0) elastic cross section is substituted for the current-weighted (P1) total scattering cross section and the average scattering cosine ($\bar{\mu}$) is assumed to be unchanged by self-shielding.

5. Both NJOY and MINX relax their linearization tolerances for small cross sections. Neither code will seek to meet the linearization tolerance if the absolute difference between the linearly interpolated cross section and the correct value is less than 10^{-5}. Because NJOY uses a unionized energy grid, it will sometimes place extra energy points in regions where MINX would not. The resulting discrepancies are not very important.

Further work is contemplated toward understanding these and other differences between the two codes. However, the results of this comparison have strengthened our confidence in the new NJOY processing system.

E. LTSS Version of NJOY (R. M. Boicourt and R. E. MacFarlane)

The NJOY nuclear cross-section processing system has been successfully converted to the LTSS time-sharing system. Many of the changes were rather minor, such as modifying the overlay commands and the logical bit manipulation routines. Obtaining efficient input/output was the major problem. The binary I/O routines in the ORDER library are very inefficient. Most users code around this problem by using BUFFERIN and BUFFEROUT or other specialized routines. However, NJOY is required to be easily converted to other systems; therefore, we wanted to keep the standard FORTRAN read and write statements. For this reason, we wrote an I/O package called ZIO that intercepts the ORDER binary read and write calls and converts them into buffer operations. The system uses double buffering in LCM, handles up to 16 separate files, automatically reads and writes families of files, and supports a skip forward-or-backward by N records capability.

In order to make it easier for T2 users of NJOY to submit jobs to the remote batch system for night runs or even to ORDER for day runs, a simple program called T2RUN has been written that generates an ORDER input file from simple CROS-like commands. The file retrieval routines automatically handle such complexities as converting from CROS form to LTSS, XPORT calls, and packing out

families of files. Output options such as CBT and microfiche are supported, and interactive input is available if desired. The following example is an input session for NJOY.

```
T2RUN / 1 1.01345

 ENTER YOUR USER NUMBER, PROGRAM RUN TIME (MINUTES), LCM REQUIRED (K).
       (I5,1X,I3,I4)
? 66749   2 300

 ENTER YOUR NAME AND COST CODE (A10,1X,A4).
? R. BOICOURT C138

 ENTER AN INPUT LINE.
? GET FS=NJOY,AC=T02,LTSS

 ENTER AN INPUT LINE.
? GET FS=C12IN AC=T02 LTSS

 ENTER AN INPUT LINE.
? GET FS=C12P,AC=T02NJOY,DEV=HP,LOCAL=21

 ENTER AN INPUT LINE.
? GET FS=T408 AC=T02DWM DEV=HP LOCAL=20

 ENTER AN INPUT LINE.
? EXECUTE FS=NJOY INPUT=C12IN

 ENTER AN INPUT LINE.
? OUTPUT FS=TAPE40 ID=GROUPR - C-12

 ENTER AN INPUT LINE.
? END

ORDERINV= GIVEN TO DEFERRED BATCH SYSTEM.
ORDERINV= SUBMITTED TO DEFERRED BATCH SYSTEM.      S 01/09/78  16:04:00
```

The "LTSS" in the GET command tells the system that the file is in LTSS rather than CROS format; the other options are as in the CROS PHOTOR command. The ORDER input file required to do the same job follows.

```
 1  $BATCH US 066749 T00 01 00 02 0300
 2  *ID    9502C138                                  R. BOICOURT     BOX T02
 3  *XEQ XPORT
 4  *XEQMES T02     GET NJOY
 5  *NXT
```

```
 6  *XEQ XPORT
 7  *XEQMES= T02      GET C12IN
 8  *NXT
 9  *XEQ XPORT
10  *XEQMES T02NJOY   GET C12P      , HP
11  *NXT
12  *XEQ CRSCNV
13  *XEQMES C12P      TAPE21A
14  *NXT
15  *XEQ DESTROY
16  *XEQMES C12P
17  *NXT
18  *XEQ XPORT
19  *XEQMES T02DWM    GET T408      , HP
20  *NXT
21  *XEQ CRSCNV
22  *XEQMES T408      TAPE20A  C.
23  *NXT
24  *XEQ DESTROY
25  *XEQMES T408
26  *NXT
27  *XEQ NJOY
28  *XEQMES C12IN
29  *NXT
30  *XEQ ALLOUT
31  *XEQMES TAPE40    BOX T02 R.BOICOURT GROUPR - C-12
32  *NXT
33  *END
```

The simplificiation is clear.

F. MATXS Self-Shielding Cross Sections (R. E. MacFarlane)

The new MATXS format is being developed to provide a generalized and comprehensive mechanism for storing multigroup-neutron, photon-production, and photon-interaction cross sections for the CCCC interface system.[36] A utility code TRANSX is used to form tables for transport codes including such options as coupled sets,

collapse to a subset group structure, and the construction of special activity edit cross sections. This system is now being extended to include self-shielded cross sections.

In the past, self-shielding data has been stored as "f-factors," the ratios of the cross sections at several values of T and σ_0 to that at some reference temperature (usually 0 K) and infinite dilution. Any use of the data requires that the reference cross section and the f-factor both be retrieved. MATXS, on the other hand, uses the "$\Delta\sigma$" method. The reference case is the first T and σ_0 for a given isotope; all subsequent sets are differences between the cross sections at that T and σ_0 and the other reference case.

This organization simplifies data handling and reduces memory requirements for many self-shielding operations. For example, to shield the total scattering matrix, the elastic $\Delta\sigma$ matrix is simply added to the reference total matrix. There is no need to retrieve the various partial cross sections required by the f-factor method. Zero $\Delta\sigma$ values (and small ones) are automatically removed from the file by the banding capabilities of MATXS for efficient use of disk space. The MATXSR module of NJOY has been modified to produce $\Delta\sigma$ MATXS files.

A new version of TRANSX is being developed that can produce self-shielded transport tables at specified values of T and σ_0, or which can use heterogeniety principles and σ_0 iterations to produce tables for specified geometries and mixtures. One new feature of the coding is a two-dimensional Lagrangian interpolation scheme using all T and σ_0 values on the MATXS library. All neutron-scattering matrices and photon-production matrices can also be shielded. The output is compatible with many existing transport and diffusion codes.

The MATXS file and this advanced version of TRANSX are the nucleus of a new space and energy self-shielding code under development at LASL.

G. Code Comparisons (R. E. MacFarlane and R. B. Kidman)

Because of the importance of validated computer codes for nuclear design, the United States Department of Energy (DOE) sponsors a Code Comparison Working Group consisting of representatives from industry and the national laboratories. LASL chairs the Processing Code Subcommittee of this group. The members have each analyzed two simple homogeneous problems based on a typical fast-breeder reactor composition using their own codes, and we have analyzed the results and tabulated comparisons. Our results were presented to the subcommittees at a meeting in Germantown on November 2, 1977. The following is a brief summary of the results.

Table VII gives a comparison of several important integral properties. Larger differences are seen between fluxes, adjoints, and cross sections. A detailed analysis of the differences between LASL and Argonne National Laboratory (ANL) showed the following major sources of differences: the use of coarse groups (1/2 lethargy in some regions) and an inappropriate weight function (1/E + fission), inadequate correction for coarse flux effects on elastic removal, and different self-shielding effects in the unresolved region (probably due to the new inclusion of same-sequence overlap correction in MC^{2}2).[37] Table VIII breaks down the Δk difference between LASL and ANL in order to show the part of the difference due to each of the important effects.

H. Interlab Doppler Comparison (R. B. Kidman)

The Processing Code Subcommittee of the Code Evaluation Working Group Group decided to compare Doppler calculation on their ZPR67 infinite homogeneous system.

LASL's preliminary Doppler results are presented in Table IX. The eigenvalues were computed first with all materials at 0 K and then with all materials at 2100 K. The eigenvalue differences are proportional to the Doppler effect. We have included more calculations than called for in order to quantify the effects that number of downscattering groups, original weighting function differences, and buckling have on the Doppler effect. The number of downscattering groups and different weighting functions have less than 1% effect on the Doppler. However, the Doppler effect for the buckled case is $\sim$34% less than for the unbuckled case. This suggests that the Committee should include the buckled Doppler case as an important variation. If no errors are discovered, we intend to report the top and bottom line results to the Committee.

I. Elastic Removal F-Factors and Spectral Adjustment Schemes (R. B. Kidman)

For most library group structures now in use, elastic outscatter of a group sensitively depends on the flux near the bottom of the group. If the actual intragroup flux shape differs greatly from that assumed by the multigroup averaging code, then special spectral corrections have to be applied to the elastic removal cross sections.

We have been investigating several iterative schemes for performing these spectral corrections, and we have applied them all to the simple reactor system specified by the Processing Code Subcommittee so we could compare each scheme to the ANL results.

TABLE VII

INTEGRAL PARAMETER COMPARISON

	ZPR-6-7 Infinite Homogeneous Medium		ZPR-6-7 Buckled Homogeneous Medium	
Parameter	ANL Value	LASL PD	ANL Value	LASL PD
K	1.2096	0.17	1.0040	0.19
C28/F49	0.1666	-0.51	0.1585	-0.26
C28/F25	0.1477	-0.60	0.1447	-0.35
F49/F25	0.8865	-0.08	0.9132	-0.12
F28/F25	0.0172	0.58	0.0206	0.68
F40/F25	0.1582	0.34	0.1806	0.33
F41/F25	1.2926	0.34	1.2943	0.33

TABLE VIII

EFFECTS OF CROSS-SECTION DIFFERENCES

Material	Differences	Eigenvalue Effect As % of Total ΔK
Mix	Absorption	-158
	$\nu\cdot$Fission	677
	Elastic Removal	-332
	Inelastic Transfer	87
^{239}Pu	Absorption	-123
	Resolved Region $\nu\sigma_f$	- 45
	Unresolved Region $\nu\sigma_f$	330
^{238}U	Resolved Region Absorption	132
	Unresolved Region Absorption	- 40
	Smooth Region Absorption	- 74
	Smooth Region $\nu\cdot$Fission	286
	Elastic Removal	102
Ni	Elastic Removal	83
Fe	Elastic Removal	-257
Cr	Elastic Removal	- 74
^{16}O	Elastic Removal	-243

TABLE IX

ZPR-6-7 HOMOGENEOUS MEDIUM DOPPLER CALCULATIONS

	$B^2 = 0$			$B^2 = 0.00073$		
Codes/Library	K at 300 K	K at 2100 K	K	K at 300 K	K at 2100 K	K
MINX[a]/1DX[b]/LIB-IV[c] full matrix[d]	1.2116	1.1805	-0.0312	1.0059	0.9853	-0.0206
MINX/1DX/LIB-IV 10 downscatter[d]	1.2121	1.1811	-0.0310	1.0061	0.9857	-0.0204
MINX/1DX/72-Gp[e] 30 downscatter[d]	1.2116	1.1804	-0.0312			
ETOX[f]/1DX 10 downscatter[d]	1.2108	1.1804	-0.0304	1.0053	0.9850	-0.0203

[a] Ref. 33

[b] Ref. 38

[c] Ref. 34

[d] These terms refer to the number of groups retained to describe the scattering from any group.

[e] A 72-Grp library (which has more high and low-energy groups than LIB-IV) was generated to test weighting function effects.

[f] Ref. 39

Sample results for the iron elastic removal cross section are compared in Table X. (Our 50-group cross sections were collapsed to the 28-group results presented in Table X for direct comparison with the ANL results.) The first column is the ANL elastic removal cross section in b. The second column is the percent deviation (PD) of the original 1DX[38] results from the ANL results. The third column shows the percent deviations obtained when no iteration on the elastic removal cross section is performed; that is, the elastic removal cross section was simply taken to be the product of the MINX[34] elastic removal cross section times the MINX elastic scattering f-factor. The fourth column represents results from a slight modification[40] of the original 1DX method. Instead of interpolating on the produce of $\xi \sigma_e \phi$ as is done in 1DX, we interpolate on the collision density, $\Sigma_t \phi$, to find the "correct" flux to use in our elastic removal definition. The last column shows results from a method[41] in which we give simplified shapes to the old and new spectra, to the elastic cross section, and to the outscatter probability. We then perform group averaging integrations to find the elastic removal changes caused by gross-spectral changes.

The eigenvalue deviations are shown along the bottom of the table to provide some idea of the magnitude of eigenvalue changes that may occur in evolving to an improved elastic removal treatment.

TABLE X

IRON ELASTIC REMOVAL CROSS-SECTION COMPARISON
ON THE ZPR-6-7 INFINITE HOMOGENEOUS MEDIUM

I	ANL Value (b)	Original 1DX with Collision 1DX PD	NIFF=0 PD	Density PD	Non-Linear PD
1	0.0701	62.4	-12.3	- 0.5	-10.5
2	0.0843	59.3	3.4	50.4	24.0
3	0.1271	4.0	-23.5	- 3.4	-13.3
4	0.1401	- 6.5	-26.4	- 6.3	-14.0
5	0.1869	5.5	-43.1	20.4	-11.5
6	0.2475	-29.6	-23.3	-34.4	-30.8
7	0.1329	67.6	-12.2	- 9.6	- 6.0
8	0.3519	-19.9	7.5	5.0	6.1
9	0.1942	25.7	- 3.5	- 1.8	- 3.1
10	0.1802	71.7	-30.3	-40.0	-34.3
11	0.3968	5.6	15.3	9.1	12.0
12	0.2114	248.3	-63.4	-65.6	-62.9
13	0.1284	16.1	13.9	14.6	4.9
14	0.3872	19.3	15.1	17.4	5.7
15	0.3877	25.5	5.3	- 3.4	- 3.6
16	0.2089	117.1	45.9	13.3	10.8
17	1.3256	-10.3	-29.3	-32.2	-13.5
18	0.5950	- 3.5	3.2	- 3.9	1.1
19	0.5536	0.2	9.6	- 2.5	- 2.5
20	0.5195	0.3	18.0	- 1.9	- 2.5
21	0.6279	-16.3	12.1	0.3	- 6.5
22	0.5389	5.1	49.9	1.7	- 7.9
23	0.3042	76.1	167.4	90.2	18.7
24	0.2866	84.1	183.9	84.3	- 2.7
25	0.2620	130.4	210.6	130.6	116.9
26	0.5850	-14.8	39.1	-13.4	-19.6
27	0.0169	- 9.4	83.5	-17.8	-79.2
28	0.000	0.0	0.0	0.0	0.0
K	1.2096	0.17	1.22	0.57	0.84

Unfortunately, it appears none of the schemes do a significantly better job than any other. Up to this point, all schemes have attempted to make corrections without requiring knowledge of resonance structure and location. This nicety may have to be abandoned because the final scheme may require the passing along of some minimum amount of resonance information.

Self-shielding factors for elastic-scattering transfer cross sections have been neglected in the past. They simply were never computed. Their generation and use were never considered, probably because of the increased amount of data required and doubts about the improvement that could result from their use.

Departing from this tradition, elastic removal f-factors have been generated with NJOY[42] for ^{16}O, ^{23}Na, Fe, ^{235}U, ^{238}U, and ^{239}Pu. Following the necessary code modifications, these f-factors were tested in our present problem. Indeed, as Table XI shows, the resulting elastic removal f-factors, FD, are a good deal different than the elastic scattering f-factors, FE, that have previously been used.

With the elastic removal f-factors incorporated, Table X becomes Table XII. The elastic removal f-factors have essentially no effect on the original 1DX scheme because after the first iteration, the elastic removal cross sections are computed independently from the elastic removal cross sections and f-factors that were input. Noticeably, however, for the other schemes, the large differences in groups 11 and 13 were corrected. Beyond that, there is no forceful trend to indicate which scheme, if any, is approaching reality.

The addition of the removal f-factors has not cleared up the Table X troubles. Spectral corrections schemes will have to be re-examined.

III. FISSION PRODUCTS AND ACTINIDES: YIELDS, YIELD THEORY, DECAY DATA, DEPLETION, AND BUILD-UP

A. Fission Yield Theory [R. E. Pepping (University of Wisconsin), D. E. Madland, C. W. Maynard (University of Wisconsin), T. R. England, and P. G. Young]

It has been determined that a combination of Gauss-Legendre and Gauss-Laguerre quadrature integration[43] rules may be used to evaluate the integrals necessary to compute yields. Cases typifying extreme behavior of the integrands were tested and gave computational accuracy of 6 parts in 10^4 in the worst instance.

Yields have been computed for a variety of assumptions on a 20 x 20 grid of ϵ shape parameters. The grid coordinates correspond to the midline of the

TABLE XI

ELASTIC SCATTERING AND REMOVAL F-FACTOR COMPARISON

	O=16		NA=23		FE		U=235		U=238		PU=239	
GP	FE	FD	FE	FD	FE	FD	FE	FD	FE	FD	FE	FD
1	.99841	1.00885	.99979	1.00131	.99804	.97860	1.00000	1.00000	.99993	.99736	1.00000	.99955
2	.99525	1.00554	.99866	.99163	.99901	.98882	1.00000	.99996	.99858	.97892	.99985	.99662
3	.97237	.92493	.99800	.98617	.99864	1.00578	1.00003	.99999	.99962	.99217	.99994	.99878
4	.95326	1.05641	.99526	.97678	.99262	1.02471	1.00000	.99997	.99971	1.01586	.99994	1.00247
5	.98420	.96492	.99480	1.00553	.97456	.98399	1.00200	.99997	.99992	1.00683	.99999	1.00168
6	.95838	.95186	.99355	.97168	.96318	.94464	1.00000	.99999	.99962	.98896	.99995	.99850
7	.99434	.94559	.97364	1.11146	.94572	.92248	1.00000	.99997	.99920	.98330	.99987	.99740
8	.93937	.97217	.99177	.97428	.97075	.93311	1.00000	1.00001	.99988	.99419	.99998	.99922
9	.99693	1.01133	.99814	1.00025	.94413	.96685	1.00000	.99999	.99981	.99256	.99998	.99691
10	.99998	1.00114	.97525	.93493	.93813	.97153	1.00000	.99999	.99987	.99234	.99998	.99896
11	1.00000	.99981	.99197	1.01804	.91570	.79027	1.00000	1.00000	.99992	.99706	.99998	.99967
12	1.00000	.99966	.99986	.99787	.92366	.82248	1.00000	1.00000	.99993	.99400	.99999	.99908
13	1.00000	.99958	1.00343	.99861	.83450	.99418	1.00000	1.00000	.99991	.99377	.99999	.99928
14	1.00000	.99966	.99972	.99922	.98345	.89546	.99999	1.00000	.99995	.99585	.99999	.99924
15	1.00000	.99970	.99999	.99873	.73433	1.15780	1.00000	1.00001	.99998	.99709	.99999	.99927
16	1.00000	.99978	.84040	.71145	.98726	.91840	1.00000	1.00001	.99999	.99757	1.00000	.99939
17	1.00000	.99980	.96693	1.03338	.99650	.98070	1.00000	1.00001	.99267	.98089	1.00000	.99949
18	1.00000	.99985	1.00087	.99925	.97655	.85020	1.00000	1.00001	.97859	.97615	1.00000	.99958
19	1.00000	.99991	1.00042	.99929	.57553	1.78228	1.00001	1.00002	.97828	.97339	1.00002	.99995
20	1.00000	.99989	.99998	.99884	.99348	.97533	1.00000	.99995	.95127	.94361	.99959	.99890
21	1.00000	.99992	.99996	.99777	.99819	.98050	1.00000	.99993	.94628	.93873	.99947	.99895
22	1.00000	.99994	.99992	.99676	.99902	.97877	1.00000	1.00002	.93138	.92210	.99918	.99848
23	1.00000	.99995	.99981	.99488	.99184	.92685	1.00000	1.00001	.91271	.90205	.99878	.99743
24	1.00000	.99997	1.00022	.99903	.95730	1.03127	1.00000	1.00003	.91589	.90445	.99884	.99846
25	1.00000	.99997	.99864	.98490	.98690	1.10552	1.00001	1.00002	.88607	.87330	.99779	.99587
26	1.00000	.99998	.99237	.95537	1.00062	.99383	1.00001	.99996	.86204	.84812	.99672	.99640
27	1.00000	.99999	.92646	.82002	.99795	1.01544	1.00002	1.00003	.85781	.99570	.99676	.99718
28	1.00000	1.00000	.82254	.71386	1.00090	.99816	1.00004	1.00005	.95029	.98854	.99694	.99728
29	1.00000	1.00000	.81349	1.21007	1.00058	.99510	1.00003	.99998	.76128	1.02279	.99359	.99611
30	1.00000	.99999	.98505	1.05843	1.00106	.99061	1.00002	.99997	.59033	.36672	.98651	.99176
31	1.00000	.99999	.99884	1.21563	1.00099	.99054	1.00001	1.00001	.69980	.28976	.96445	.97759
32	1.00000	.99999	.99992	1.00571	.99304	1.01940	.99997	.99997	.59810	.99083	.96823	.92920
33	1.00000	.99999	1.00006	1.00256	.99984	.99081	.99996	.99977	.60355	1.03658	.97115	.97171
34	1.00000	1.00000	1.00005	1.00098	.99993	.99340	.99994	.99987	.61368	1.06661	.95018	.82686
35	1.00000	1.00000	1.00000	1.00050	.99996	.99481	.99993	.99986	.71620	1.02092	.88970	1.00298
36	1.00000	1.00000	1.00000	1.00030	.99998	.99654	.99994	.99989	.92814	.98225	.97028	.93354
37	1.00001	1.00000	1.00001	1.00020	.99999	.99794	.99992	.99968	.58367	.98916	.91622	.81291
38	1.00001	.99999	1.00001	1.00034	.99998	.99876	.99971	.99995	.24671	1.12090	.89322	.92378
39	1.00001	1.00000	1.00001	1.00016	.99999	.99913	.99972	.99938	.22322	.03564	.84051	1.02790
40	1.00002	1.00000	1.00001	.99999	1.00001	.99978	.99982	.99431	.27531	1.07782	.77517	1.02427
41	1.00005	1.00000	1.00002	1.00000	1.00002	.99978	.99969	.98075	.88425	.37573	.73256	1.17985
42	1.00007	1.00000	1.00007	.99999	1.00003	.99967	.99898	.99230	.08524	.94842	.98681	.93405
43	1.00008	1.00000	1.00011	.99997	1.00004	.99965	.99780	1.00049	.17906	1.09479	.86497	1.12194
44	1.00010	1.00000	1.00014	.99987	1.00004	.99951	.99827	.97986	.99957	.97089	.90326	1.13135
45	1.00005	.99999	1.00019	.99981	1.00004	.99947	.99992	.98716	.38686	1.28953	.95461	1.07784
46	1.00023	.99999	1.00028	.99971	1.00003	.99907	1.00008	.99947	.99898	.99866	.99993	.99447
47	1.00002	.99999	1.00059	.99969	1.00002	.99887	1.00054	.99879	.99888	.99784	1.00033	.98549
48	1.00001	.99998	1.00082	.99971	1.00001	.99884	.99991	.99714	.99882	.99902	1.00099	.97815
49	1.00001	.99998	1.00096	.99974	1.00001	.99906	1.00032	.99623	.99998	.99933	.99986	.95604
50	1.00000	1.00000	1.00064	1.00000	1.00003	1.00000	.99991	1.00000	1.00007	1.00000	1.00006	1.00000

TABLE XII

IRON ELASTIC REMOVAL CROSS-SECTION COMPARISON
ON THE ZPR-6-7 INFINITE HOMOGENEOUS MEDIUM

I	Value (b)	Original 1DX with Collision: 1DX PD	Original 1DX with Collision: NIFF=0 PD	Original 1DX with Collision: Density PD	Non-Linear PD
1	0.0701	62.4	-13.2	0.6	-11.1
2	0.0843	59.3	4.2	49.0	24.0
3	0.1271	4.0	-21.1	0.7	-10.2
4	0.1401	- 6.5	-25.7	- 5.2	-13.0
5	0.1869	5.6	-44.2	17.3	-13.5
6	0.2475	-29.7	-25.2	-36.6	-32.8
7	0.1329	67.6	- 6.0	- 2.5	0.9
8	0.3519	-19.9	- 6.8	- 8.3	- 7.6
9	0.1942	25.8	13.0	17.2	13.5
10	0.1802	71.8	7.1	- 4.8	1.6
11	0.3968	5.7	9.2	5.5	6.5
12	0.2114	248.0	7.6	0.7	8.4
13	0.1284	16.1	11.9	12.4	3.8
14	0.3872	19.3	8.1	9.2	- 0.9
15	0.3877	25.6	18.6	9.4	8.6
16	0.2089	16.7	56.2	29.4	21.5
17	1.3256	-10.4	-33.5	-31.7	-17.8
18	0.5950	- 3.5	4.3	- 4.1	3.2
19	0.5536	0.2	9.6	- 2.2	- 2.9
20	0.5195	0.3	17.7	- 1.9	- 2.5
21	0.6279	-16.3	11.3	- 0.5	- 7.1
22	0.5389	5.1	49.5	5.3	- 6.9
23	0.3042	76.1	167.2	76.6	25.8
24	0.2866	84.1	183.9	86.2	-31.9
25	0.2620	130.3	210.5	121.1	116.9
26	0.5850	-14.8	39.1	-13.1	-24.0
27	0.0169	- 9.4	86.2	-14.3	-37.0
28	0.0000	0.0	0.0	0.0	0.0
K	1.2096	0.17	1.31	0.72	0.95

20 x 5 grid in ε, ε_4-space employed by Seeger and Howard[44] and usually corresponds to an ε_4-value of zero. This choice was made to simplify computation. A shape-dependent yield was computed for each possible $\varepsilon^{(1)}$ and $\varepsilon^{(2)}$ pair. Yield grids have been calculated for two values of δ, the Coulomb parameter described previously,[45] and two other models of density parameter a in addition to that reported previously.[46] The first is the original model (described in Ref. 47), which we have determined by the same fitting procedure as reported previously,[46] to be given by a = 0.3A. The second is of the form proposed by Gilbert and Cameron[13] and is given by a = A (0.258 + 0.00974S).

Four treatments of the resulting yield grid have been employed.

1. The shape-yield spectrum is assumed to be a delta-function at the shape corresponding to the maximum value of the G-function[45] and is integrated over shape (G_{max} method).

2. The shape-yield distribution is assumed to be given by a delta-function at the shape corresponding to that of the maximum of the shape-dependent yield and is integrated over shape (Y_{max} method).

3. The shape distribution is assumed to be given by a Gaussian with its peak located at the point of maximum shape-dependent yield and widths determined by the adjacent points and is integrated over shape (Gauss method).

4. No shape distribution is assumed; the shape integration is performed by a simple sum over all gird points (Sum method).

For each resulting fragment yield, the effect of prompt neutrons are taken into account in a simple way to determine the product yield. This is done by assuming that if neutron emission is energetically possible, it occurs. The neutrons are assumed to have either no kinetic energy or 2.0 MeV of kinetic energy. When neutron emission is no longer energetically possible, the remaining energy is assumed to appear as prompt gamma rays. Neutron separation energies for this calculation are taken from Ref. 44. The energy available for prompt neutrons and gammas is obtained by summing the energy from fragment excitation, and the energy to be recovered as the fragment shape relaxes to the ground-state shape. Also, for one case, an attempt has been made to improve the mass formula by assuming the ground-state mass to be given by Garvey-Kelson mass relations as reported by Janecke in Ref. 48, and by measured values where such data exist. The yield calculation is quite sensitive to the mass, and the Garvey-Kelson relations show a RMS deviation of 118 keV when compared to measured masses, whereas the Seeger-Howard formula[44] shows a RMS deviation of 704 keV. The

Seegar-Howard formula is then used to determine masses relative to the ground state for other shapes.

The results (Table XIII) are surprisingly insensitive to the treatment of the yield grid, with only the peak-to-valley ratio showing any real variation. Unfortunately, it appears to deteriorate as the amount of detail put into the parameter a is increased. The onset of symmetry for the case of δ = 3.5 fm may be understood by noting that the dominant effect of increasing δ is to reduce the Coulomb energy, which in turn increases the value of the G-function. The effect is then similar to that of increasing the neutron bombarding energy with the resulting reduction in the peak-to-valley ratio. Other consistent deviations from experimental observation are the absence of a dip in the total kinetic energy in the region of symetric fission and the fact that the prompt neutrons appear to be emitted primarily by the heavy fragment rather than a "saw-tooth" distribution from both fragments. The experimental observations are summarized in Ref. 49.

The mass distributions are only slightly different than those obtained in a similar statistical model calculation.[50] The mass-peak shift seems to be a recurring feature of statistical model predictions. Of interest with the current version of the model is the effect of pairing upon the yields along a given mass chain. Good experimental results have recently been reported[51] for the case of thermal fission of ^{235}U. The present model may be of some use in predicting this effect where experimental data are unavailable.

B. ENDF/B-V Yields (T. R. England, N. L. Whittemore, W. B. Wilson, and D. G. Madland)

Two codes were written to produce the ENDF/B-V yields, including all data required for an extended, revised format. These data include 20 sets each of independent and cumulative (by A and Z) yields and associated uncertainties. A total of 44 120 yields are included. The independent yields are direct fission yields before delayed neutron emission, and the cumulative yields are summations for each Z value along each mass chain after delayed neutron emission. Copies of the yields have been sent to Brookhaven National Laboratory (BNL) for incorporation into the ENDF/B-V actinide file.

Following data testing, these yields will be revised as necessary to assure consistency with the decay data file and to incorporate any new data. Special edits of half-lives and branching ratios were prepared and sent to the Chairman of the Decay Data Subcommittee.

TABLE XIII

YIELD CALCULATION SENSITIVITY STUDIES

a-Model Ref. No	δ (fm)	Mass	Method	T_n(MeV)	$\bar{\nu}_p$	$\bar{\gamma}$ (MeV)	$\bar{Q}$ (MeV	P_L	P_H	P_L/V
47	2.44	Seeger	Y_{max}	0	2.64	5.8	203	100	131	1500
47	2.44	Seeger	Gauss	0	1.58	4.6	198	100	135	10^5
22	2.44	Seeger	Y_{max}	0	3.05	7.0	202	102	131	650
22	2.44	Seeger	G_{max}	0	3.05	7.0	202	102	131	4350
22	2.44	Seeger	Gauss	0	3.02	6.5	202	102	131	1125
46	2.44	Seeger	Y_{max}	0	2.6	6.8	200	102	130	5
46	2.44	Seeger	G_{max}	0	2.7	6.8	200	102	132	8
46	2.44	Seeger	Gauss	0	2.5	6.3	200	102	132	2
46	2.44	Seeger	Gauss	2	1.6	9.0	200	102	132	3.6
46	2.44	Garvey	Y_{max}	0	2.9	7.2	200	102	130	31
46	2.44	Garvey	G_{max}	0	2.8	7.0	200	102	131	42
46	2.44	Garvey	Gauss	0	2.8	6.7	200	102	132	27
46	2.44	Garvey	Sum	0	2.3	8.2	201	102	132	28
46	3.5	Seeger	Y_{max}	0	3.3	6.7	200	118	118	1
46	3.5	Seeger	G_{max}	0	3.2	6.2	199	118	118	1
46	3.5	Seeger	Gauss	0	3.1	7.0	199	118	118	1

EXPLANATION:

a-Model = level density parameter described in given reference.

δ = Coulomb parameter.

Mass = formula given by Seeger – Howard[44] or by Seeger – Howard with Garvey-Kelson correction to ground-state mass as reported by Janecke in Ref. 48.

Method = Treatment of shape-dependent yield grid (see text).

T_n = prompt neutron kinetic energy assumed.

$\bar{\nu}_p$ = spectrum averaged number of prompt neutrons.

$\bar{\gamma}$ = spectrum averaged total energy appearing in prompt gamma rays.

$\bar{Q}$ = spectrum averaged reaction total energy release.

P_L = location of fission-product light mass peak.

P_N = location of fission-product heavy mass peak.

P_L/V = ratio of yield at P_L to that in symmetric valley.

It should be noted that ENDF/B-V yield evaluations and files differ from ENDF/B-IV values in the following respects:

1. The number of yield sets has doubled and the cumulative yields are now included.
2. Uncertainties are now incorporated in the files.
3. Yields are given before and after delayed neutron emission (i.e., for the independent and cumulative yields, respectively).
4. The yield distribution models for pairing and isomeric states (Refs. 52 and 53) are now incorporated.
5. Recent, and in some cases unpublished, experimental data have been incorporated.
6. The final yields will also incorporate ternary fission in conserving the fissionable nuclide charge. The model of Ref. 54 will be used.

The file data has been expanded by a factor of 8, including the uncertainties.

C. Delayed Neutron Calculations (T. R. England, W. B. Wilson, and N. L. Whittemore)

The ENDF/B-V yield data evaluations include only two conservation principles: the yield summations under each mass peak are normalized to 100%, and the fissionable nuclide charge is conserved by adjusting the Z_p value (the most probable charge yielded per mass chain). This leaves several parameters available that can be used in checking the overall quality of the yields, such as the Q-value per fission, prompt neutons per fission, and total number of delayed neutrons $\bar{\nu}_d$ per fission.

$\bar{\nu}_d$, calculated from the yields, is particularly sensitive to the model parameters used in distributing the mass-chain yields. The calculated $\bar{\nu}_d$ also depends on the neutron emission probabilites Pn of delayed precursors.

As noted in the last progress report[55] there are now 69 known precursors, 48 have measured Pn values and, based on energetics, there are a total of $\sim$102 probable precursors. Most of the prominant precursors are included in the 48 measured Pn values, and all probable precursors have model estimated values. All values were tabulated in Ref. 55.

These Pn values and the preliminary ENDF/B-V yields have been used to calculate the number of delayed neutrons for each of the 102 precursors for each yield set and the total $\bar{\nu}_d$ per yield set. The total $\bar{\nu}_d$ results are tabulated in Table XIV along with some experimental data and ENDF/B evaluations.

TABLE XIV

DELAYED NEUTRONS[a] PER 100 FISSIONS

Fissionable Nuclide	Calculated From Preliminary ENDF/B-V Data		Evaluation ENDF/B-IV[b]	Range of Experimental Data[c]	
^{232}Th(F)	4.66	(4.35)	5.27 ± 0.40	3.9 ± 0.9	5.9 ± 1.5
^{232}Th(H)	3.23	(2.89)	3.00 ± 0.40	1.30 ± 0.51	8.72 ± 0.67
^{233}U(T)	0.825	(0.773)	0.740±0.04	0.63 ± 0.18	0.671± 0.041
^{233}U(F)	0.895	(0.839)	0.740 ± 0.04	0.67 ± 0.08	0.75 ± 0.064
^{233}U(H)	0.636	(0.585)	0.44 ± 0.05	1.42 ± 0.42	0.439± 0.04
^{235}U(T)	1.72	(1.59)	1.67 ± 0.07	1.58 ± 0.10	2.05 ± 0.61
^{235}U(F)	1.90	(1.74)	1.67 ± 0.07	1.63 ± 0.13	1.83 ± 0.18
^{235}U(H)	1.04	(0.947)	0.90 ± 0.10	0.88 ± 0.07	0.91 ± 0.04
^{236}U(F)	2.22	(2.00)	---	---	---
^{238}U(F)	3.31	(2.84)	4.60 ± 0.25[d]	3.88 ± 0.49	4.84 ± 0.36
^{238}U(H)	2.59	(2.22)	2.60 ± 0.20	1.70 ± 0.67	7.85 ± 0.50
^{237}Np(F)	1.22	(1.07)	---	---	-
^{239}Pu(T)	0.743	(0.638)	0.645± 0.04	0.59 ± 0.23	0.95 ± 0.15
^{239}Pu(F)	0.696	(0.572)	0.645± 0.04	0.62 ± 0.05	0.721_ 0.008
^{239}Pu(H)	0.446	(0.367)	0.43 ± 0.03	0.41 ± 0.02	1.35 ± 0.16
^{240}Pu(F)	0.855	(0.720)	0.90 ± 0.09	0.94 ± 0.11	---
^{241}Pu(T)	1.51	(1.24)	1.57 ± 0.15	0.160± 0.16	---
^{241}Pu(F)	1.39	(1.12)	1.57 + 0.15	--	---
^{242}Pu(F)	1.32	(1.09)	---	1.50 ± 0.5	---
^{252}Cf(S)	0.633	(0.472)	---	0.86 ± 0.10	---

[a] Values in parentheses include only measured Pn values (48 nuclides); otherwise the calculations include model estimates for an additional 54 precursors. (NOTE: T = Thermal, F = Fast, H = High Energy, and S = Spontaneous Fission.)

[b] Evaluations and uncertainties from S. A. Cox, "Delayed Neutron Data - Review and Evaluation," Argonne National Laboratory report ANL/NDM-5 (1974).

[c] Summary report by R. J. Tuttle, "Delayed Neutron Data for Reactor-Physics Analysis," Nucl. Sci. Eng. 56, 37 (1975).

[d] Preliminary ENDF/B-V evaluation alters this to 4.40 ± 0.12.

D. Library for Processed ENDF/B Aggregate Fission-Product Spectra (R. J. LaBauve, T. R. England, and D. George)

PEFPYD is a library of processed ENDF/B aggregate fission-product spectra and yield data in an ENDF-like format. The format, structure, and contents of the library have been described in previous progress reports.[55,56] Also described were codes for collapsing the data in the library into coarser energy groups and fitting the results along the cooling time (t) axis with linear combinations of functions of the type

$$fc(t) = \sum_{i=1}^{n} \alpha_i e^{-\lambda_i t} \quad .$$

In Ref. 57 a technique is described for applying a fitted "pulse" spectra (irradiation time = 10^{-4} s) to the calculation of decay power after a finite irradiation time. In order to check the validity of this technique, analytic fits accurate to 0.5% were made to an 11-group structure from the PEFPYD 150 fine-group structure for a ^{235}U thermal pulse, and beta spectra for the broad-group structure were calculated for a case for which ^{235}U fuel was irradiated with thermal neutrons for 20 000 h These spectra were then compared with those calculated directly with the CINDER-10 code for the same case.

This comparison revealed that although the approximate calculation agreed to within 3% with CINDER-10 for the sums over the energy bins of the beta-decay energies for various cooling times, large differences of +31 and -77% were seen for the low- and high-energy groups, respectively, for the shortest cooling time (0.1 s). For cooling times greater than 100 s, the comparison was within the expected accuracy (5%). This indicated that the normalization used for constructing cumulative spectra, which include those fission products in ENDF/B-IV for which spectral data are not given, was inadequate. For this normalization, it is assumed that the fission products for which there are no spectral data yield the same cumulative spectral shape as those 181 for which spectral data are given in ENDF/B-IV. Spectral data for short-lived fission products are particularly sparse in ENDF/B-IV. The suspicion that this assumption is not adequate for generating finite spectra from pulse data was confirmed by rerunning the problems but limiting the comparison to the 181 nuclides with spectra. The fit to the burst for this case was made to an accuracy of 1.5%, and the individual spectra now agreed with CINDER-10 results to within 3.0% for each cooling time. Examples of the comparison for all fission products and for the 181 fission products having spectra are in Table XV.

TABLE XV

20 000 h THERMAL IRRADIATION OF ^{235}U (% DIFFERENCE BETWEEN CINDER-10 AND APPROXIMATE METHOD)

Cooling Time (s)	Group 1.0.1-0.4 MeV		Group 5,1.8-2.2 MeV		Group 10,5.0-6,0 MeV	
	All F.P.	181 F.P.	All F.P.	181 F.P.	All F.P.	181 F.P.
1.0 E-01	30.7	-0.3	-3.1	0.1	-63.4	-0.5
1.0 E+00	27.5	-0.3	-3.1	0.2	-59.4	-0.7
1.0 E+01	19.3	-0.2	-3.0	0.2	-50.1	-1.2
1.0 E+02	6.8	-0.1	-0.6	0.6	- 7.1	3.7
1.0 E+03	2.0	0.3	0.3	0.4	5.5	1.1
1.0 E+04	1.0	0.7	0.6	0.4	0.2	1.3
1.0 E+05	0.7	0.6	-0.5	0.5	1.3	0.1
1.0 E+06	1.5	1.6	-0.4	-0.4	-	-
1.0 E+07	1.5	1.5	0.0	0.2	-	-
1.0 E+08	-4.1	-4.1	0.1	-0.4	-	-
1.0 E+09	0.1	0.1	0.0	0.0	-	-

Because of shown normalization difficulty, a scheme has been devised for constructing approximate individual beta and gamma spectra for the fission products in ENDF/B-IV having no spectral data. The beta (or gamma) spectrum for a particular nuclide is constructed by assuming the spectrum shape of the aggregate 181 nuclides from a pulse after a cooling time approximately equal to the half-life of the nuclide in question. This shape is then normalized to the average beta (gamma) decay energy of the nuclide. Figs. 14 and 15, respectively, compare the gamma and beta spectra of ^{139}Cs with those constructed for a hypothetical nuclide having the same half-life and average gamma- and beta-decay energies as ^{139}Cs. The nuclide ^{139}Cs is a relatively important nuclide in the 0.1 s cooling time bin for 20 000 h thermal irradiation of ^{235}U. However, it should be noted that such constructed individual spectra will be used only in the aggregate. This work is still in progress.

E. Multigroup and Few-Group Cross Sections for ENDF/B-IV Fission Products (W. B. Wilson, T. R. England, and R. J. LaBauve)

A library of 154-group cross sections, processed with the NJOY[42] code from the ENDF/B-IV fission product data library, was produced as an intermediate product in the production of a four-group library for a version of the CINDER fission-

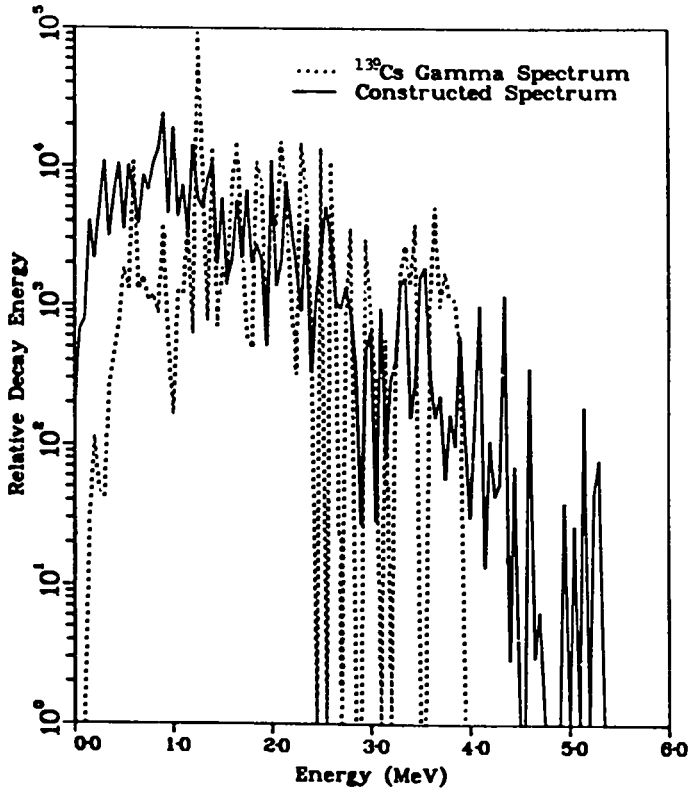

Fig. 14.
^{139}Cs gamma spectrum compared with constructed spectrum.

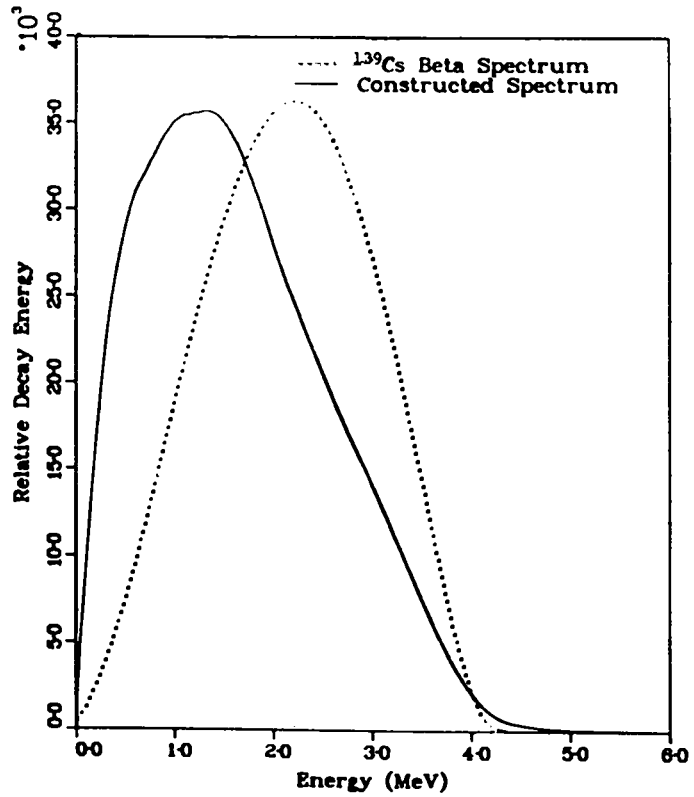

Fig. 15.
^{139}Cs beta spectrum compared with constructed spectrum.

product absorption and depletion code.[58,59] The TOAFEW cross-section collapsing code, developed and used locally to produce few-group values, and the 154-group library have been refined to facilitate their application by other users.

A file of the code and library will soon be released to the National Neutron Data Center. A LASL report describing the code and library is in preparation.

F. Preliminary Examination of the Gunst, Connor, and Conway Experiments as A Potential Benchmark for Fission-Product Absorption in Thermal Reactors (W. B. Wilson and T. R. England)

1. Description of Experiment. The experiments of Gunst, Connor, and Conway constitute the most extensive measurements of fission-product absorption in thermal reactors available.[60,61] In these experiments, samples of ^{233}U and natural thorium were irradiated to high depletion in consecutive 3-wk cycles in the Materials Testing Reactor (MTR) and Advanced Test Reactor (ATR). Three-group flux histories during irradiation cycles were obtained from flux monitors. Reactivity measurements following most of the irradiation cycles were made on each sample in the Advanced Reactivity Measurement Facility (ARMF-I). The analytical model called TARMPF was used to extract fission-product absorption parameters from the measured sample reactivities using calculated actinide reactivity contributions and fission history. These absorption parameters were transformed to associated parameters appropriate to the MTR for comparison with calculated parameters specific to the irradiation facility.

The neutron-energy group structure of the irradiation flux history was determined by the flux spectrum description adapted for the MTR. This description incorporated a thermal Maxwellian distribution at 343.2 K extending from 0 to infinite energy, a 1/E epithermal distribution above 0.105 eV, plus some augmentation for fission-spectrum neutrons. Three-group microscopic absorption and fission cross sections for actinide nuclides in the MTR group structure (0, 0.105 eV, 5.53 keV, 10 MeV) are given in Ref. 59 along with coefficients of a density dependent exponential self-shielding treatment. Similar data are given for microscopic absorption cross sections of moderator, structural, and fission-product nuclei.

Reactivity measurements were conducted in the ARMF-I with samples positioned at various locations in a central water hole and in fuel elements surrounding the water hole. The neutron-flux spectrum of the water hole in general was described by a Maxwellian distribution at 299.6 K with a 1/E distribution

added above 0.120 eV. The slightly harder neutron spectrum characteristic of fuel element locations was described by a Maxwellian distribution at 315.6 K with a 1/E distribution added above 0.098 eV. Associated with each region of the ARMF-I is a microscopic cross section-tabulation, similar to that for the MTR, reflecting the different spectra and group structure (the upper limit of the thermal group being, in each case, the lower limit of the 1/E distribution).

Reactivity measurements and TARMF model calculations combined to produce values of the thermal fission-product absorption cross section $\hat{\sigma}_3$ and epithermal fission-product absorption cross section $\hat{\sigma}_2$ for the measurement location. The caret (^) is used to indicate units of b/fis. The epithermal value $\hat{\sigma}_2$ tacitly includes all fast absorption. All values of $\hat{\sigma}_3$ and $\hat{\sigma}_2$ resulting from individual measurements were transformed to associated values appropriate to a reference water-hole location, and a number of measurements were conducted at a variety of ARMF-I measurement positions to form a single set of fitted values of $\hat{\sigma}_3$ and $\hat{\sigma}_2$ for the reference water-hole position for the irradiation/cooling time history.

These resulting values of $\hat{\sigma}_3$ and $\hat{\sigma}_2$ were then transformed to cross-section values appropriate to the MTR spectrum. These values are the effective 2200 m/s thermal cross section ($\hat{\sigma}_{2200}$), the resonance integral above 0.105 eV (I), and an effective 1-group cross section ($\hat{\sigma}_{eff}$) that, when multiplied by the effective 2200 m/s flux (ϕ_{2200}), accurately reproduces the total fission-product absorption.

The limitations on the resulting values of $\hat{\sigma}_2$, $\hat{\sigma}_3$, $\hat{\sigma}_{2200}$; I, and $\hat{\sigma}_{eff}$ are as follows:

(a) Data used in the TARMF model calculations and transformations to the reference water-hole location did not originate from the data library used in benchmark calculations.

(b) Simplifying assumptions are required in the ARMP transformations and transformation to the MTR.[58,59]

(c) The tacit inclusion of fast absorption in $\hat{\sigma}_2$ complicates the one-to-one correspondence of "measured" and calculated parameters.

2. LASL Calculations of the Experiment. The Electric Power Research Institute (EPRI) is currently funding the Nuclear Data Group T-2 of LASL to examine this and other experiments as potential fission-product benchmarks. The results of one of the Gunst et al. experiments (sample 46) has been calculated using the 4-group EPRI-CINDER code and fission-product data library.[58,59] This library resulted from the collapsing of a 154-group library reflecting a light-water

TABLE XVI

MEASURED AND CALCULATED VALUES OF $\hat{\sigma}_{2200}$, Sample 46

Irradiation Cycle	Elapsed Time (h)	(Barns/Fission) BAPL Values Measured	BAPL Values Calculated	LASL Calculated Values 4-Gp (LWR)	LASL Calculated Values 3-Gp (MTR)	LASL Calculated Values 3-Gp (ARMF)
2	1641.12	128.0 ± 6.4	124.7	127.11	127.92	119.66
3	2719.87	105.2 ± 5.3	101.8	103.44	105.31	98.74
4	3490.08	183.4 ± 9.2	192.1	171.26	187.86	176.07
4	3706.08	81.0 ± 4.0	90.6	89.95	92.42	86.85
7	5619.46	67.2 ± 3.4	71.1	69.77	72.63	68.54
8	6388.68	90.6 ± 4.5	95.5	88.40	95.70	90.28
8	6775.68	61.5 ± 3.1	67.6	66.43	69.21	65.40
10	8045.58	54.6 ± 2.7	59.7	59.66	62.27	58.98
12	9369.95	62.3 ± 3.1	69.2	64.02	68.77	65.19
12	9716.95	49.0 ± 2.5	56.6	54.71	57.15	54.22
14	11057.24	46.9 ± 2.4	52.2	50.28	52.46	49.87
17	12807.80	47.6 ± 2.4	52.3	48.59	51.83	49.38
17	13200.80	39.8 ± 2.0	46.2	44.19	46.21	44.06
21	15913.79	42.1 ± 2.1	46.9	43.35	45.90	43.81
21	16244.79	37.2 ± 1.9	42.3	40.37	41.84	39.96
22	17708.61	35.2 ± 1.8	40.6	38.95	40.32	38.52
23	18683.63	35.6 ± 1.8	38.1	37.26	38.64	36.96
24	19378.63	37.1 ± 1.9	43.1	39.70	42.10	40.23
24	19839.63	36.7 ± 1.8	38.0	36.15	37.55	35.93
25	22368.50	37.1 ± 1.9	41.5	38.25	40.46	38.68
25	22777.50	33.1 ± 1.7	36.7	35.05	36.26	34.72
25	25399.50	32.9 ± 1.7	36.2	34.84	36.50	34.95

TABLE XVII

MEASURED AND CALCULATED VALUES OF $\hat{I}$, Sample 46

Irradiation Cycle	Elapsed Time (h)	(Barns/Fission) BAPL Values		LASL Calculated Values		
		Measured	Calculated	4-Gp (LWR)	3-Gp (MTR)	3-Gp (ARMF)
2	1641.12	248.1 ± 17.4	196.4	212.50	224.51	218.34
3	2719.87	162.9 ± 11.4	196.8	200.56	218.37	213.66
4	3490.08	246.2 ± 17.2	220.8	237.83	232.23	228.51
4	3706.08	262.0 ± 18.3	195.6	192.62	213.08	209.25
7	5619.46	201.0 ± 14.1	185.3	175.44	196.54	194.01
8	6388.68	207.2 ± 14.5	193.3	185.58	199.93	198.06
8	6775.68	221.8 ± 15.5	184.1	173.20	193.46	191.23
10	8045.58	210.1 ± 14.7	177.8	165.51	185.40	183.60
12	9369.95	194.1 ± 13.6	176.4	164.17	179.93	178.78
12	9716.95	209.8 ± 14.7	170.9	158.52	176.33	174.88
14	11057.24	180.9 ± 12.7	164.6	151.95	168.80	167.62
17	12807.80	177.2 ± 12.4	158.8	145.65	159.75	159.15
17	13200.80	182.8 ± 12.8	155.2	142.64	157.30	156.53
21	15913.79	168.2 ± 11.8	148.0	136.04	148.01	147.59
21	16244.79	175.0 ± 12.3	144.9	133.72	146.01	145.43
22	17708.61	175.2 ± 12.3	141.6	130.73	142.41	141.88
23	18683.63	148.3 ± 10.4	138.7	127.90	139.21	138.78
24	19378.63	170.6 ± 11.9	138.9	128.09	138.20	137.93
24	19839.63	133.4 ± 9.3	136.0	125.44	136.06	135.68
25	22368.50	159.6 ± 11.2	135.8	125.29	134.81	134.58
25	22777.50	147.7 ± 10.3	133.1	122.88	132.90	132.57
25	25399.50	149.4 ± 10.5	132.4	122.40	131.61	131.37

TABLE XVIII

MEASURED AND CALCULATED VALUES OF $\hat{\sigma}_{eff}$, Sample 46

Irradiation Cycle	Elapsed Time (h)	(Barns/Fission) BAPL Values		LASL Calculated Values		
		Measured	Calculated	4-Gp (LWR)	3-Gp (MTR)	3-Gp (ARMF)
2	1641.12	185.6 ± 5.6	170.3	155.77	180.37	170.67
3	2719.87	143.2 ± 4.3	147.7	132.56	156.51	148.84
4	3490.08	241.0 ± 7.2	243.8	200.10	242.58	229.93
4	3706.08	142.4 ± 4.3	136.4	119.19	142.68	136.21
7	5619.46	114.1 ± 3.4	114.3	97.97	118.81	114.14
8	6388.68	138.8 ± 4.2	140.5	116.25	142.65	136.80
8	6775.68	113.1 ± 3.4	110.5	94.36	114.65	110.32
10	8045.58	103.1 ± 3.1	100.7	86.59	105.43	101.73
12	9369.95	106.7 ± 3.2	109.5	89.94	110.27	106.42
12	9716.95	96.9 ± 2.9	95.6	80.58	97.82	94.56
14	11057.24	88.0 ± 2.6	89.7	75.24	91.24	88.38
17	12807.80	87.6 ± 2.6	88.2	72.33	88.29	85.70
17	13200.80	81.1 ± 2.4	81.2	67.84	82.11	79.80
21	15913.79	80.0 ± 2.4	80.3	65.74	79.66	77.47
21	16244.79	76.6 ± 2.3	75.0	62.64	75.15	73.13
22	17708.61	74.6 ± 2.2	72.5	60.74	72.72	70.80
23	18683.63	69.0 ± 2.1	69.3	58.69	70.33	68.55
24	19378.63	75.5 ± 2.3	74.4	60.90	73.59	71.65
24	19839.63	66.7 ± 2.0	68.6	57.23	68.56	66.86
25	22368.50	73.1 ± 2.2	72.1	59.06	71.19	69.35
25	22777.50	66.4 ± 2.0	66.7	55.74	66.56	64.94
25	25399.50	66.5 ± 2.0	66.0	55.46	66.50	64.90

TABLE XIX

MEASURED AND CALCULATED ARMF-I VALUES OF $\hat{\sigma}_1$, $\hat{\sigma}_2$ AND $\hat{\sigma}_3$, Sample 46

Irradiation Cycle	Elapsed Time (h)	$\hat{\sigma}_3$ (Barns/Fission)		$\hat{\sigma}_2$ (Barns/Fission)		$\hat{\sigma}_1$ (Barns/Fission)
		BAPL Measured	LASL 3-Gp (ARMF) Calculated	BAPL Measured	LASL 3-Gp (ARMF) Calculated	LASL 3-Gp (ARMF) Calculated
2	1641.12	112.18	104.976	22.52	19.489	.19530
3	2719.87	92.20	86.628	14.69	19.176	.19709
4	3490.08	160.74	154.469	22.09	20.104	.19560
4	3706.08	70.99	76.199	24.03	18.835	.19763
7	5619.46	58.90	60.135	18.41	17.525	.19611
8	6388.68	79.40	79.207	18.88	17.775	.19558
8	6775.68	53.90	57.372	20.37	17.284	.19670
10	8045.58	47.85	51.740	19.31	16.613	.19516
12	9369.95	54.60	57.190	17.79	16.129	.19331
12	9716.95	42.94	47.570	19.31	15.830	.19389
14	11057.24	41.10	43.749	16.63	15.181	.19217
17	12807.80	41.72	43.321	16.28	14.397	.18965
17	13200.80	34.88	38.657	16.84	14.184	.18995
21	15913.79	36.90	38.435	15.47	13.355	.18687
21	16244.79	32.60	35.056	16.13	13.177	.18700
22	17708.61	30.85	33.794	16.15	12.855	.18598
23	18683.63	31.20	32.427	13.65	12.576	.18510
24	19378.63	32.52	35.291	15.72	12.478	.18424
24	19839.63	32.16	31.525	12.25	12.294	.18435
25	22368.50	32.52	33.935	14.69	12.176	.18340
25	22777.50	29.01	30.459	13.60	12.012	.18348
25	25399.50	28.83	30.662	13.76	11.899	.18343

reactor flux spectrum. Simplifying assumptions were required for the four-group representation of the reported three-group flux history and actinide cross-section data. (The principle assumptions are that the aggregate fission-product absorption is 1/v, and the flux is 1/E in the energy region of 0.105-0.625 eV.)

Additional calculations for the same sample have recently been performed with a three-group library produced by collapsing the 154-group data to the MTR flux spectrum and group structure. In addition to the calculation of the reported values with the data (3-group MTR), nuclide number densities produced in these calculations have been combined with yet another 3-group library collapsed to the flux spectrum and group structure of the ARMF-I reference water hole position. The resulting calculated values of $\hat{\sigma}_3$ $\hat{\sigma}_2$, and $_1$ (3-group ARMF) were used to construct the MTR values of ($\hat{\sigma}_{2200}$, I, and $\hat{\sigma}_{\hat{}eff}$ in much the same fashion of that used in Ref. 59. In addition, values of σ_3 and σ_2 associated with the ARMF were extracted from the reported values of $\hat{\sigma}_{2200}$, I, and $\hat{\sigma}_{eff}$ and compared to the corresponding calculated values.

Measured and calculated values of $\hat{\sigma}_{2200}$, I, and $\hat{\sigma}_{eff}$ are compared in Tables XVI, XVII, and XVIII, respectively. The measured and calculated values of $\hat{\sigma}_3$, $\hat{\sigma}_2$, and $\hat{\sigma}_1$ are compared in Table XIX.

REFERENCES

1. H. Schroder, K. K. Kern, F. Schmidt, and D. Fick, "Investigation of A = 5 Levels Strongly Coupled to the Nucleus $^4He^*$(0+) Channel," Nucl. Phys. A269, 74 (1976).

2. J. C. Hopkins, D. M. Drake, and H. Conde, "Elastic and Inelastic Scattering of Fast Neutrons from ^6Li and ^7Li," Nucl. Phys. A107, 139 (1968).

3. D. G. Gardner and Yu-Wen Yu, "Trends in Nuclear Cross Sections," Nucl. Phys. 60, 49 (1964).

4. I. Kimura, K. Kobayashi, and T. Shibata, "Measurements of Average Cross Sections for Some Threshold Reactions with Fission-Type Reactor Spectra," Nucl. Sci. Tech. 8, 59 (1971).

5. D. Wilmore and P. E. Hodgson, "The Calculation of Neutron Cross Sections from Optical Potentials," Nucl Phys. 55, 673 (1964).

6. F. G. Perey, "Optical Model Analysis of Proton Elastic Scattering in the Range of 9 to 22 MeV," Phys. Rev. 131, 745 (1963).

7. Lynne McFadden and G. R. Satchler, "Optical Model Analysis of the Scattering of 24.7 MeV Alpha Particles," Nucl. Phys. 84, 177 (1964).

8. D. M. Brink, thesis, Oxford University (1955); P. Axel, "Electric Dipole Ground State Transition Width Strength Function," Phys. Rev. 126, 671 (1962).

9. C. H. Johnson, A. Galonsky, and R. L. Kernell, "Anomalous Optical Model Potential for Sub-Coulomb Protons for $89 \leq A \leq 130$," Phys. Rev. Lett. 39, 1604 (1977).

10. J. M. Blatt and U. F. Weisskopf, Theoretical Nuclear Physics (John Wiley and Sons, Inc., New York, 1952).

11. S. F. Mughabghab and D. I. Garber, "Neutron Cross Sections, Vol. 1, Resonance Parameters," Brookhaven National Laboratory report BNL-325 (1973).

12. E. H. Auerbach and S. O. Moore, "Calculations of Inelastic Scattering of Neutrons by Heavy Nuclei," Phys. Rev. 135, B895 (1964).

13. A. Gilbert and A. G. W. Cameron, "A Composite Nuclear Level Density Formula with Shell Corrections," Can. J. Phys. 43, 1446 (1965).

14. J. L. Cook, H. Ferguson, and A. R. de L. Musgrove, "Nuclear Level Densities in Intermediate and Heavy Nuclei," Aust. J. Phys. 20, 447 (1967).

15. D. M. Drake, Los Alamos Scientific Laboratory, personal communication (1977).

16. M. Lindner, R. J. Nagle, and J. H. Landrum, "Neutron Capture Cross Sections from 0.1 to 3 MeV by Activation Measurements," Nucl. Sci. Eng. 59, 381 (1976).

17. P. G. Young and E. D. Arthur, "GNASH, A Preequilibrium, Statistical Nuclear Model Code for Calculation of Cross Sections and Emission Spectra," Los Alamos Laboratory report LA-6947 (1977).

18. C. Kalbach, "PRECO - A Programme for Calculating Preequilibrium Particle Energy Spectra," Centre D'Etudes Nucleaires de Saclay report Dph-N/BE/73/3 (1974) and personal communication (1977).

19. C. I. Baxman and P. G. Young, "Applied Nuclear Data Research and Development July 1 - September 30, 1977," Los Alamos Scientific Laboratory report LA-7066-PR, p. 14 (1977).

20. C. E. Bemis, F. K. McGowan, J. L. C. Ford, W. T. Millner, P. H. Stetsun, and R. L. Robinson, "E2 and E4 Transition Moments and Equilibrium Deformations in the Actinide Nuclei," Phys. Rev. C8, 1466 (1973).

21. P. Axel, "Electric Dipole Ground State Transition Width Strength Function," Phys. Rev. 126, 671 (1962).

22. Calculated by F. M. Mann, Hanford Engineering Development Laboratory, Personal communication to P. G. Young (December 1977).

23. L. Green and J. A. Mitchell, Proc. of Conf. on Neutron Cross Sections and Tech., Knoxville, Tennessee, Vol. 1, p. 325 (1971).

24. D. Graham Foster. Jr., and Dale W. Glasgow, "Neutron Total Cross Sections 2.5-15 MeV I. Experimental," Phys. Rev. C3, 576 (1971).

25. D. I. Garber and R. R. Kinsey, "Neutron Cross Sections, 3rd ed., Vol. II," Brookhaven National Laboratory report series BNL-325 (January 1976), and personal communication from National Neutron Cross Section Center, Brookhaven National Laboratory.

26. D. G. Madland, Los Alamos Scientific Laboratory, personal communication, 1978.

27. J. W. Behrens and G. W. Carlson, "Measurement of the Fission Cross Sections of ^{233}U and ^{239}Pu," Lawrence Livermore Laboratory report UCRL-79577 (1977).

28. J. C. Hopkins and B. C. Diven, "Neutron Capture to Fission Ratios in ^{233}U, ^{235}U, and ^{239}Pu," Nucl. Sci. Eng. 12, 169 (1962).

29. C. M. Eisenhauer, J. A. Grundl, and A. Fabry, "Neutron Transport Calculations for the Intermediate-Energy Standard Neutron Field (ISNF) at the National Bureau of Standards," Proc. of Symp. on Neutron Standards and Applications, Natl. Bur. Stand. Spec. Publ. 493 (October 1977).

30. R. B. Kidman and R. E. MacFarlane, "CINX: Collapsed Interpretation of Nuclear X Sections," Los Alamos Scientific Laboratory report LA-6287-MS (1976).

31. D. W. Muir and R. E. MacFarlane, "Collapse Theory," in "Applied Nuclear Data Research and Development January 1 - March 31, 1977," Los Alamos Scientific Laboratory report LA-6893-PR, pp. 14-17 (1977).

32. R. B. Kidman, "LIB-IV-240 Two-Hundred-Forty Group Library," in "Applied Nuclear Data Research and Development April 1 - June 30, 1976," Los Alamos Scientific Laboratory report LA-6560-PR, pp. 13-15 (1976).

33. C. R. Weisbin, P. D. Soran, R. E. MacFarlane, D. R. Harris, R. J. LaBauve, J. S. Hendricks, J. E. White, and R. B. Kidman, "MINX: A Multigroup Interpretation of Nuclear X-Sections from ENDF/B," Los Alamos Scientific Laboratory report LA-6486-MS (1976).

34. R. B. Kidman and R. E. MacFarlane, "LIB-IV, A Library of Group Constants for Nuclear Reactor Calculations," Los Alamos Scientific Laboratory report LA-6260-MS (March 1976).

35. R. Douglas O'Dell, "Standard Interface Files and Procedures for Reactor Physics Codes, Version IV," Los Alamos Scientific Laboratory report LA-6941-MS (Sept. 1977).

36. B. M. Carmichael, "Standard Interface Files and Procedures for Reactor Physics Codes, Version III," Los Alamos Scientific Laboratory report LA-5486-MS (February 1974).

37. H. Henryson II, B. J. Toppel, and C. G. Stenberg, "MC^2-2: A Code to Calculate Fast Neutron Spectra and Multigroup Cross Sections," Argonne National Laboratory report ANL-8144 (ENDF-239) (June 1976).

38. R. W. Hardie and W. W. Little, "1DX, A One-Dimensional Diffusion Code for Generating Effective Nuclear Cross Sections," Battelle Northwest Laboratory report BNWL-954 (March 1969).

39. R. E. Schenter, J. L. Baker, and R. B. Kidman, "ETOX, A Code to Calculate Group Constants for Nuclear Reactor Calculations," Battelle Northwest Laboratory report BNWL-1002 (May 1969).

40. R. B. Kidman, R. E. MacFarlane, and M. Becker, "Flux Interpolation for Elastic Downscatter," Trans. Am. Nucl. Soc., 26, 580 (June 1977).

41. R. B. Kidman, "Spectral Corrections to Elastic-Removal Cross Sections," Trans. Am. Nucl. Soc. 24, 468 (November 1976).

42. R. E. MacFarlane and R. M. Boicourt, "NJOY: A Neutron and and Photon Cross-Section Processing System," Trans. Am. Nucl. Soc. 22, 720 (1975).

43. F. Hildebrand, Introduction to Numerical Analysis (McGraw-Hill, New York, 1956), Chapter 8.

44. P. A. Seeger and W. M. Howard, "Semi-Emperical Atomic Mass Formula," Nucl. Phys A238, 491 (1975).

45. C. I. Baxman and P. G. Young, Comp., "Applied Nuclear Data Research and Development, January 1-March 31, 1977," Los Alamos Scientific Laboratory report LA-6893-PR, p. 24 (July 1977).

46. C. I. Baxman and P. G. Young, Comp., "Applied Nuclear Data Research and Development, July 1-September 30, 1977," Los Alamos Scientific Laboratory report LA-7066-PR, p. 24 (December 1977).

47. H. A. Bethe, "Nuclear Physics, B. Nuclear Dynamics, Theoretical," Rev. Mod. Phys. 9, 69 (1937).

48. A. H. Wapstra and K. Bos, "A 1975 Midstream Atomic Mass Evaluation," At. Data Nucl. Data Tables 17, 474 (1976).

49. R. Vandenbosch and J. R. Huizenga, Nuclear Fission (Academic Press, New York, 1973), Chapters 10-12.

50. B. D. Wilkins, E. P. Steinberg, and R. R. Chasman, "Scission-Point Model of Nuclear Fission Based on Deformed Shell Effects," Phys. Rev. C14, 1832 (1976).

51. H. G. Clerc et al., "The Influence of Pairing and Nuclear Structure on the Thermal-Neutron-Induced Fission of ^{235}U," IKDA 75/10 (June 1975).

52. D. G. Madland and T. R. England, "The Influence of Pairing on the Distribution of Independent Yield Strengths in Neutron-Induced Fissions," Los Alamos Scientific Laboratory report LA-6430-MS (ENDF-240) (July 1976).

53. D. G. Madland and T. R. England, "Distribution of Independent Fission-Product Yields to Isomeric States," Los Alamos Scientific Laboratory report LA-6595-MS (ENDF-241) (November 1976).

54. D. G. Madland and Leona Stewart, "Light Ternary Fission Products: Probabilities and Charge Distributions," Los Alamos Scientific Laboratory report LA-6783-MS (ENDF-247) (April 1977).

55. C. I. Baxman and P. G. Young, Comp., "Applied Nuclear Data Research and Development July 1 - September 30, 1977," Los Alamos Scientific Laboratory report LA-7066-PR (December 1977).

56. C. I. Baxman and P. G. Young, Comp., "Applied Nuclear Data Research and Development April 1 - June 30, 1977," Los Alamos Scientific Laboratory report LA-6971-PR (September 1977).

57. R. J. LaBauve, T. R. England, M. G. Stamatelatos, and D. George, "Approximations to Summation Calculations of Delayed Energy and Spectra from Fission Products," Los Alamos Scientific Laboratory report LA-6684-MS (Jaunary 1977).

58. T. R. England, W. B. Wilson, and M. G. Stamatelatos, "Fission Product Data for Thermal Reactors. Part 1 A Data Set for EPRI-CINDER Using ENDF/B-IV," Los Alamos Scientific Laboratory report LA-6745-MS (EPRI NP-356, Part 1) (December 1976).

59. T. R. England, W. B. Wilson, and M. G. Stamatelatos, "Fission Product Data for Thermal Reactors. Part 2 Users Manual for EPRI-CINDER Code and Data," Los Alamos Scientific Laboratory report LA-6746-MS (EPRI NP-356, Part 2) (December 1976).

60. S. B. Gunst, J. C. Connor, and D. E. Conway, "Measured and Calculated Fission-Product Poisoning in Neutron-Irradiated Uranium-233," Nucl. Sci. Eng. 58, 387 (1975).

61 S. B. Gunst, J. C. Connor, and D. E. Conway, "Measurements and Calculations of Heavy Isotopes in Irradiated Fuels and of ^{233}U Fission-Product Poisoning," Bettis Atomic Power Laboratory report WAPD-TM-1182 (1974).